AIAA

AIAA-2001-0806
A Validation Summary of the NCC Turbulent Reacting/Non-Reacting Spray Computations
M.S. Raju
Dynacs Engineering Company, Inc.
Brook Park, OH

39th AIAA Aerospace Sciences
Meeting & Exhibit
January 8–11, 2001 / Reno, NV

A Validation Summary of the NCC Turbulent Reacting/Non-Reacting Spray Computations

M.S. Raju
Dynacs Engineering Company, Inc., Brook Park, Ohio

Since its founding, NASA has been dedicated to the advancement of aeronautics and space science. The NASA Scientific and Technical Information (STI) Program Office plays a key part in helping NASA maintain this important role.

The NASA STI Program Office is operated by Langley Research Center, the Lead Center for NASA's scientific and technical information. The NASA STI Program Office provides access to the NASA STI Database, the largest collection of aeronautical and space science STI in the world. The Program Office is also NASA's institutional mechanism for disseminating the results of its research and development activities. These results are published by NASA in the NASA STI Report Series, which includes the following report types:

- TECHNICAL PUBLICATION. Reports of completed research or a major significant phase of research that present the results of NASA programs and include extensive data or theoretical analysis. Includes compilations of significant scientific and technical data and information deemed to be of continuing reference value. NASA's counterpart of peer-reviewed formal professional papers but has less stringent limitations on manuscript length and extent of graphic presentations.

- TECHNICAL MEMORANDUM. Scientific and technical findings that are preliminary or of specialized interest, e.g., quick release reports, working papers, and bibliographies that contain minimal annotation. Does not contain extensive analysis.

- CONTRACTOR REPORT. Scientific and technical findings by NASA-sponsored contractors and grantees.

- CONFERENCE PUBLICATION. Collected papers from scientific and technical conferences, symposia, seminars, or other meetings sponsored or cosponsored by NASA.

- SPECIAL PUBLICATION. Scientific, technical, or historical information from NASA programs, projects, and missions, often concerned with subjects having substantial public interest.

- TECHNICAL TRANSLATION. English-language translations of foreign scientific and technical material pertinent to NASA's mission.

Specialized services that complement the STI Program Office's diverse offerings include creating custom thesauri, building customized data bases, organizing and publishing research results . . . even providing videos.

For more information about the NASA STI Program Office, see the following:

- Access the NASA STI Program Home Page at *http://www.sti.nasa.gov*

- E-mail your question via the Internet to help@sti.nasa.gov

- Fax your question to the NASA Access Help Desk at 301–621–0134

- Telephone the NASA Access Help Desk at 301–621–0390

- Write to:
  NASA Access Help Desk
  NASA Center for AeroSpace Information
  7121 Standard Drive
  Hanover, MD 21076

AIAA–2001–0806

A Validation Summary of the NCC Turbulent Reacting/Non-Reacting Spray Computations

M.S. Raju
Dynacs Engineering Company, Inc., Brook Park, Ohio

National Aeronautics and
Space Administration

Glenn Research Center

December 2000

Acknowledgments

Available from

NASA Center for Aerospace Information
7121 Standard Drive
Hanover, MD 21076
Price Code: A03

National Technical Information Service
5285 Port Royal Road
Springfield, VA 22100
Price Code: A03

Available electronically at http://gltrs.grc.nasa.gov/GLTRS

A Validation Summary of the NCC Turbulent Reacting/Non-Reacting Spray Computations

M.S. Raju*

Dynacs Engineering Co., Inc.

NASA Glenn Research Center

21000 Brookpark Road

Cleveland, Ohio-44135

1 ABSTRACT

This paper provides a validation summary of the spray computations performed as a part of the NCC (National Combustion Code) development activity. NCC is being developed with the aim of advancing the current prediction tools used in the design of advanced technology combustors based on the multi-dimensional computational methods. The solution procedure combines the novelty of the application of the scalar Monte Carlo PDF (Probability Density Function) method to the modeling of turbulent spray flames with the ability to perform the computations on unstructured grids with parallel computing. The calculation procedure was applied to predict the flow properties of three different spray cases: one is a non-swirling unconfined reacting spray, the second is a non-swirling unconfined non-reacting spray, and the third is a confined swirl-stabilized spray flame. The comparisons involving both gas-phase and droplet velocities, droplet size distributions, and gas-phase temperatures show reasonable agreement with the available experimental data. The comparisons involve both the results obtained from the use of the Monte Carlo PDF method as well as those obtained from the conventional CFD solution. Detailed comparisons in the case of a reacting non-swirling spray clearly highlight the importance of chemistry/turbulence interactions in the modeling of reacting sprays. The results from the PDF and non-PDF methods were found to be markedly different and the PDF solution is closer to the reported experimental data. The PDF computations predict that most of the combustion occurs in a predominantly diffusion-flame environment. However, the non-PDF solution predicts incorrectly that the combustion occurs in a predominantly vaporization-controlled regime. The Monte Carlo temperature distribution shows that the functional form of the PDF for the temperature fluctuations varies substantially from point to point. The results also bring to the fore some of the deficiencies associated with the use of assumed-shape PDF methods in spray computations.

2 NOMENCLATURE

D_{ko}	initial drop diameter, m
g	global or gas-phase
k	droplet group or liquid phase
m_{ko}	initial mass flow rate associated with the kth droplet group
r_{ko}	initial drop radial location, m
t	time, s
u_{ko}	initial drop axial velocity component, m/s
v_{ko}	initial drop radial velocity component, m/s
w_{ko}	initial drop tangential velocity component, m/s
Δt_g	local time step in the flow solver, s
$\Delta t_{inj.}$	time step at which a new droplet group is introduced, s
Δt_k	time step used in the spray solver, s

3 INTRODUCTION

The success of any numerical tools used in multidimensional combustor modeling depends not only on the modeling and numerical accuracy considerations but also on the computational efficiency considerations as determined by the computer memory and

turnaround times afforded by the present-day computers. With the aim of developing an efficient solution procedure for use in multidimensional combustor modeling, we extended not only the scalar Monte Carlo PDF method to the modeling of turbulent reacting sprays but also the spray computations to parallel computing in order to facilitate large-scale combustor applications.[1] In this approach, the mean gas-phase velocity and turbulence fields are determined from the solution of a conventional CFD method, the scalar fields of species and enthalpy from a modeled PDF transport equation using a Monte Carlo method, and a Lagrangian-based dilute spray model is used for the liquid-phase representation. The application of this method showed reasonable agreement when detailed comparisons were made for several different cases involving both unconfined/confined and swirl/no-swirl reacting sprays.[1-3]

It is well known that considerable effort usually goes into generating structured-grid meshes for gridding up practical combustor geometries which tend to be very complex in shape and configuration. The grid generation time could be reduced considerably by making use of existing automated unstructured grid generators.[4] With the aim of advancing the current multi-dimensional computational tools used in the design of advanced technology combustors, two new computer codes - LSPRAY[5] and EUPDF[6] - were developed here, thereby extending our previous work[1] on the Monte Carlo PDF and sprays to unstructured grids as a part of the National Combustion Code (NCC) activity. The unstructured 3D solver is designed to be massively parallel and accommodates the use of an unstructured mesh with mixed elements comprised of either triangular, quadrilateral, and/or tetrahedral type. The ability to perform the computations on unstructured meshes allows representation of complex geometries with relative ease.

A current status of the the use of the parallel computing in turbulent reacting flows involving sprays, scalar Monte Carlo PDF and unstructured grids was described in Ref. 7. It also outlines several numerical techniques developed for overcoming some of the high computer time-and-storage limitations placed by the use of Monte Carlo solution methods. The parallel performance of both the PDF and CFD computations was found to be excellent but the results were mixed for the spray module showing reasonable performance on massively parallel computers like Cray T3D; but its performance was poor on the workstation clusters. In order to improve the parallel performance of the spray module, two different domain decomposition strategies were developed and the results from both strategies were summarized.[2-3,7]

In this paper, we only summarize the results of three validation cases picked to demonstrate a wide range of solutions. For a detailed description of the overall solution procedure involving both the spray and PDF solvers, the interested reader is referred to Refs. 3, 5 and 6. Refs. 2-3 and 7 provide a detailed description of the parallel performance together with the development and implementation of the parallel method. And Ref. 1 provides the results of two more validation cases.

The main objective of our present work is to show the limitations and capabilities of the NCC solution procedure in the modeling of turbulent spray computations. The calculation procedure was applied to predict the flow properties of three different spray cases: Case 1 is a reacting methanol spray with no-swirl, Case 2 is a non-reacting methanol spray with no-swirl, and Case 3 is a confined swirl-stabilized n-heptane reacting spray. The experimental data for Cases 1 & 2 were reported by McDonell and Samuelsen of the university of California, Irvine,[8] and for Case 3 by Bulzan at the NASA Glenn research center.[9] The reported measurements of McDonell and Samuelsen contained both gas-phase and droplet velocities, droplet size distributions, and gas-phase temperatures and those of Bulzan contained droplet velocities and droplet size distributions. The data of McDonell and Samuelsen's reacting spray enables us to investigate the importance of chemistry/turbulence interactions in a reacting spray. This was done by making detailed comparisons for the case of a reacting spray with two different sets of computations, one in which the solution for the temperature and species fields was obtained from the use of the scalar Monte Carlo PDF method and in the other was obtained from the solution of a conventional CFD solution.

4 RESULTS AND DISCUSSION

A General Description of Cases 1 & 2 of McDonell and Samuelsen is given in Section 4.1. The results of Case 1 are given in Sections 4.1.1 to 4.1.1.6. Sections 4.1.2 to 4.1.2.3 provide the results of Case 2. Finally, the results of Case 3 are summarized in Section 4.2.
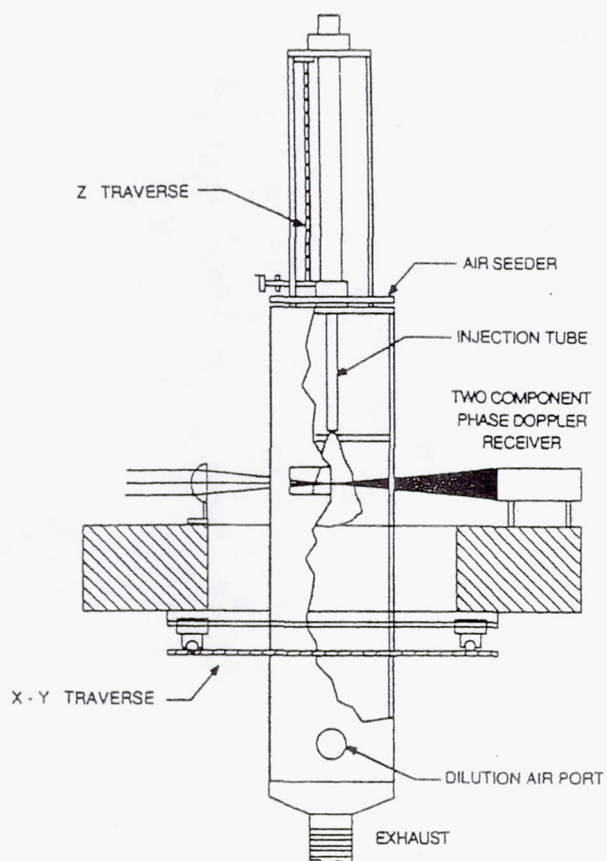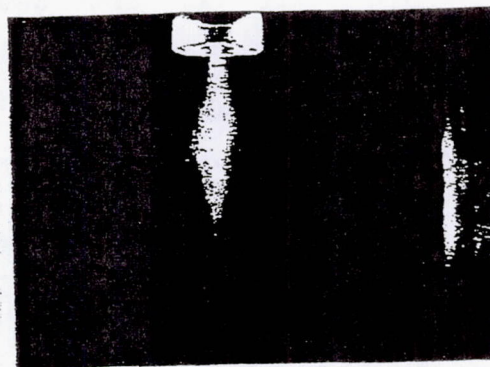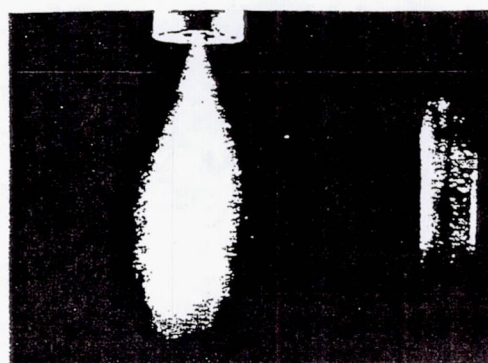
Fig. 1 Schematic of the spray burner
facility (McDonell & Samuelson).

(a) Case 1, reacting & no-swirl

(b) Case 2, non-reacting & no-swirl

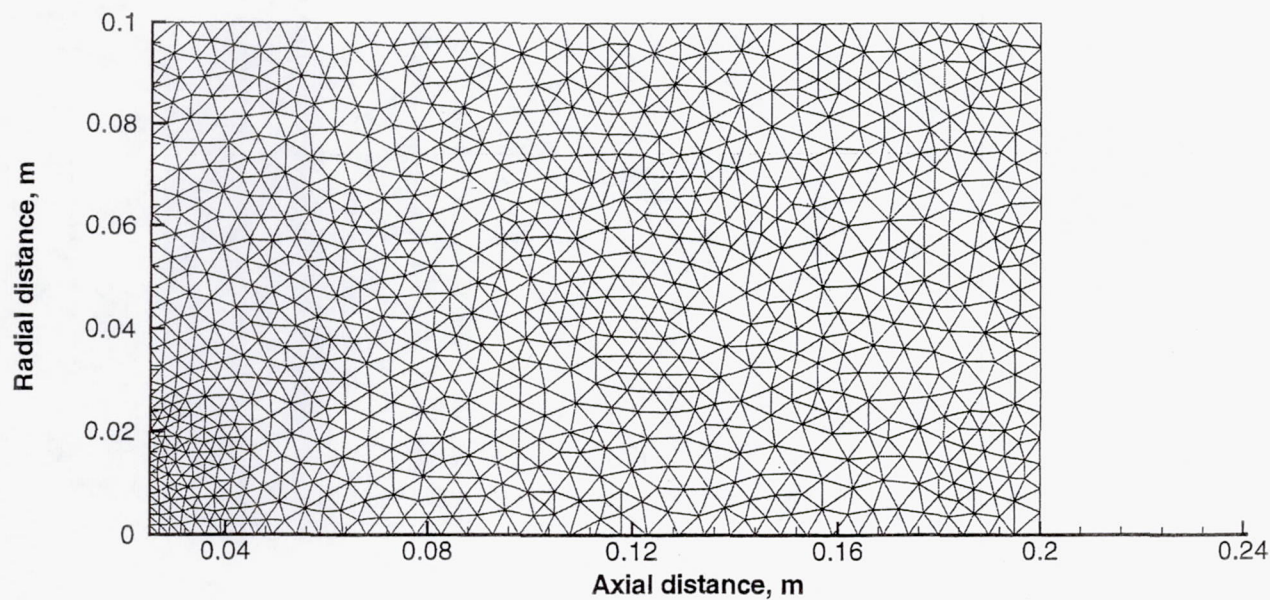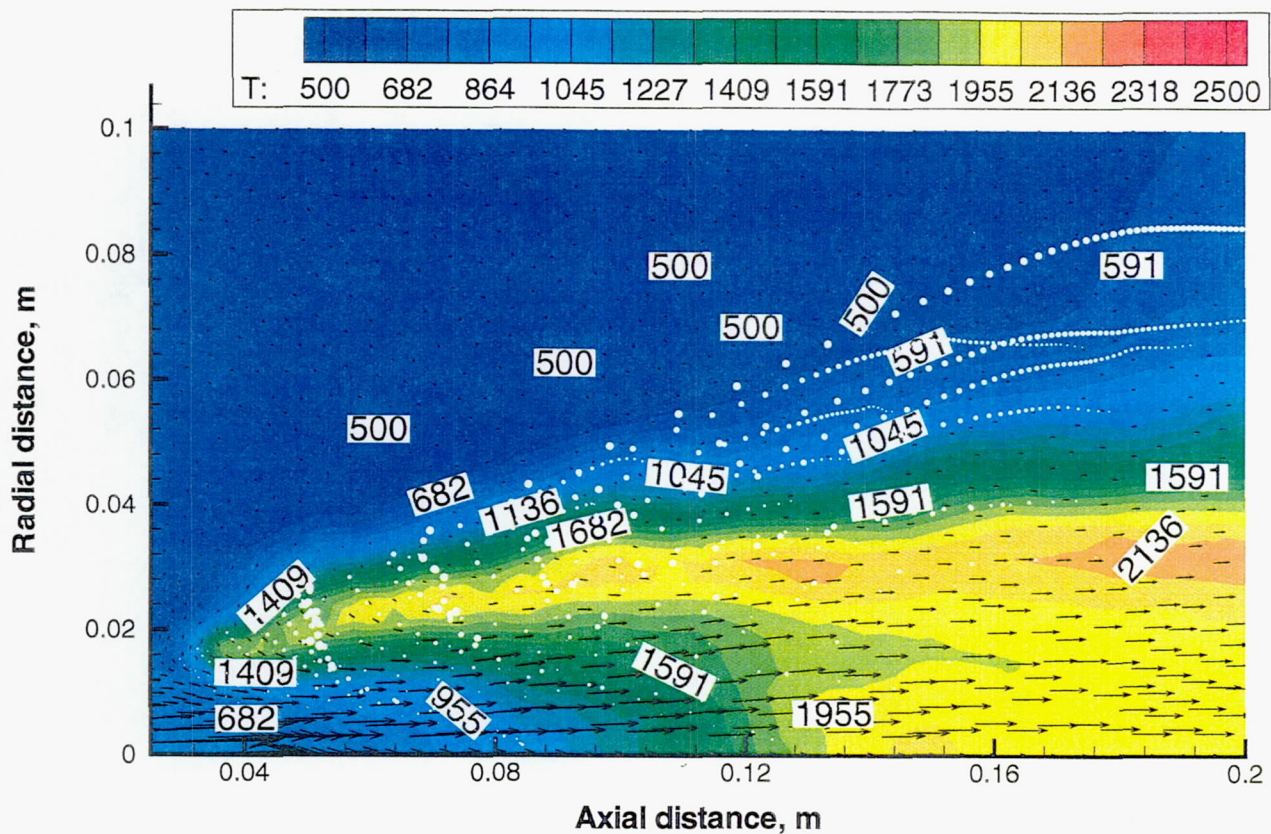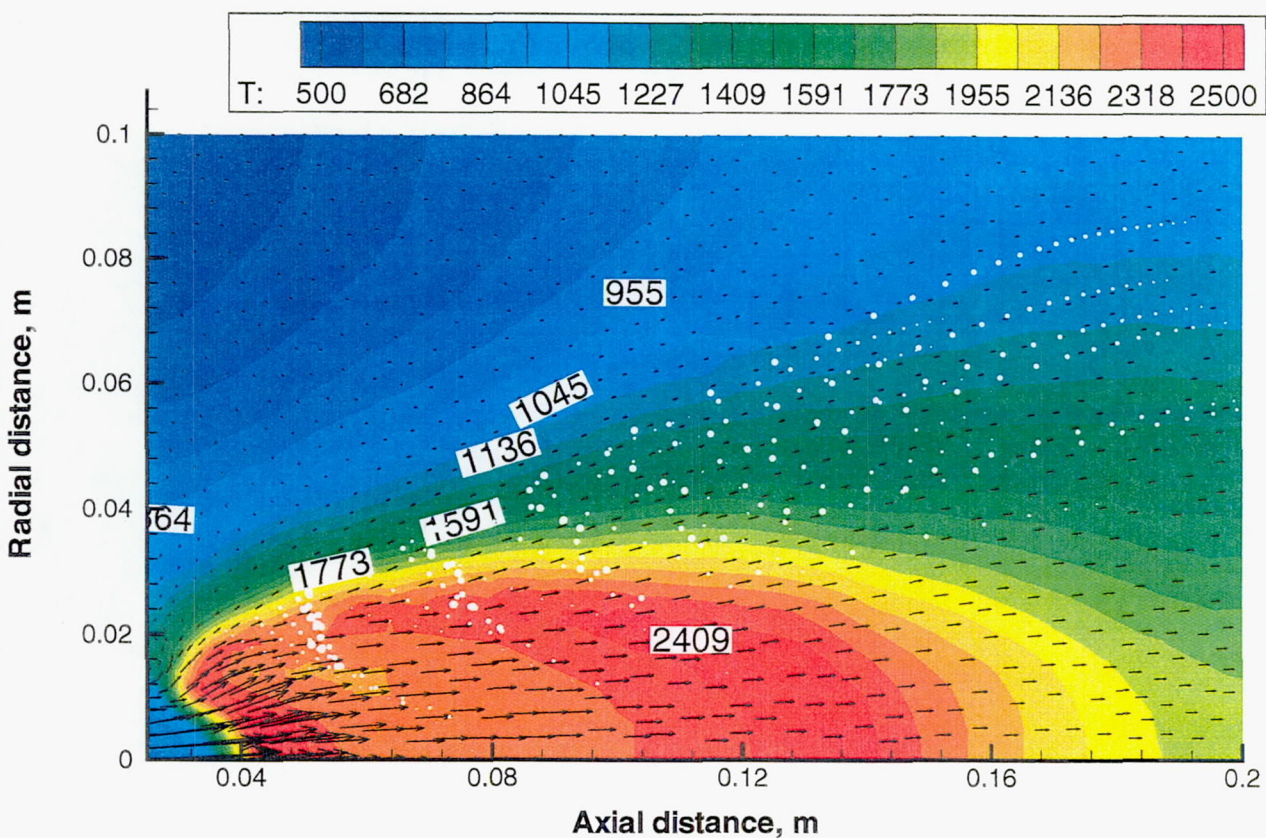Fig. 2 Backlit photographs of sprays
(McDonell & Samuelsen).

Fig. 3 2D computational grid for Cases 1 & 2 of McDonell & Samuelsen (1850 elements).

Fig. 4   The global features of a spray flame for Case 1 showing gas-phase
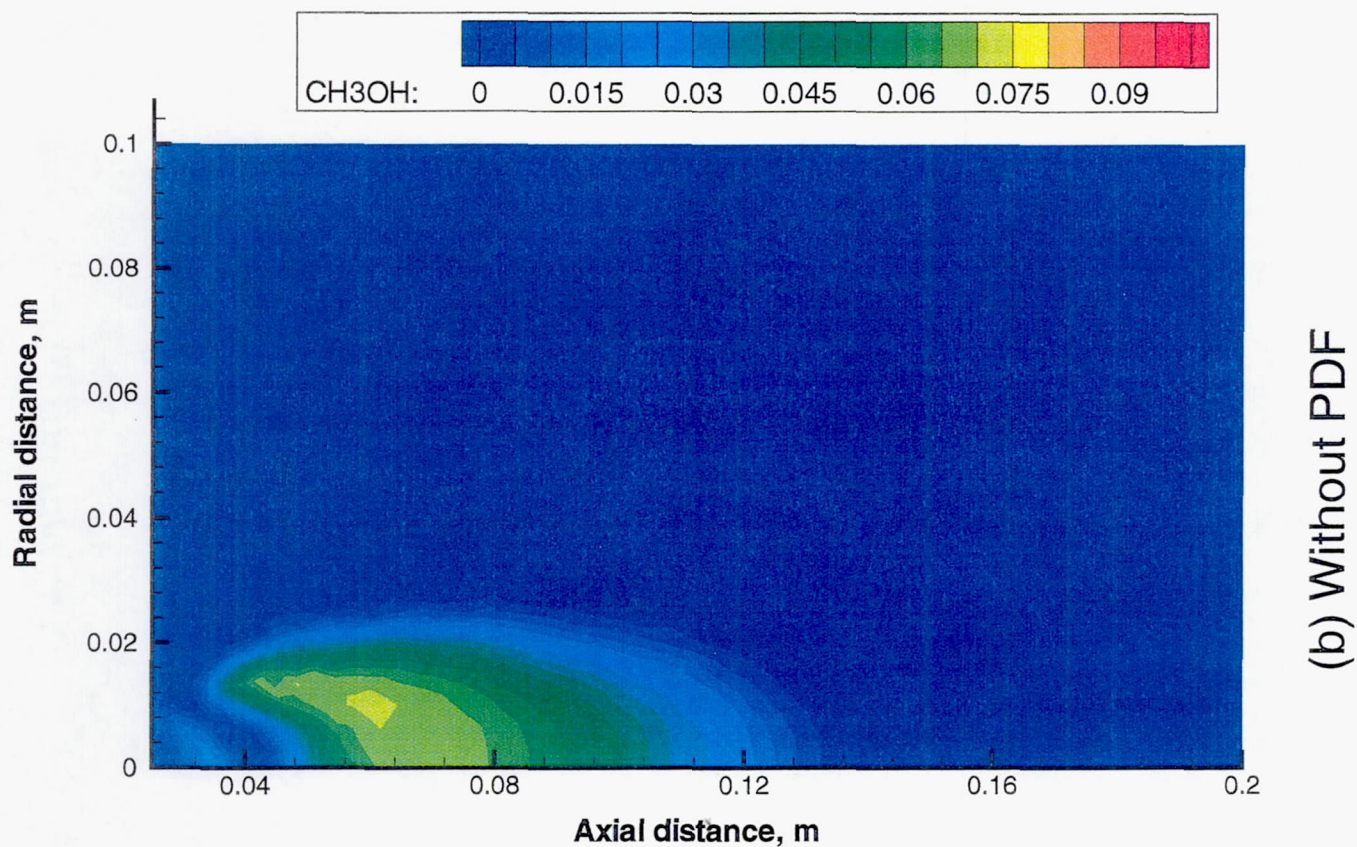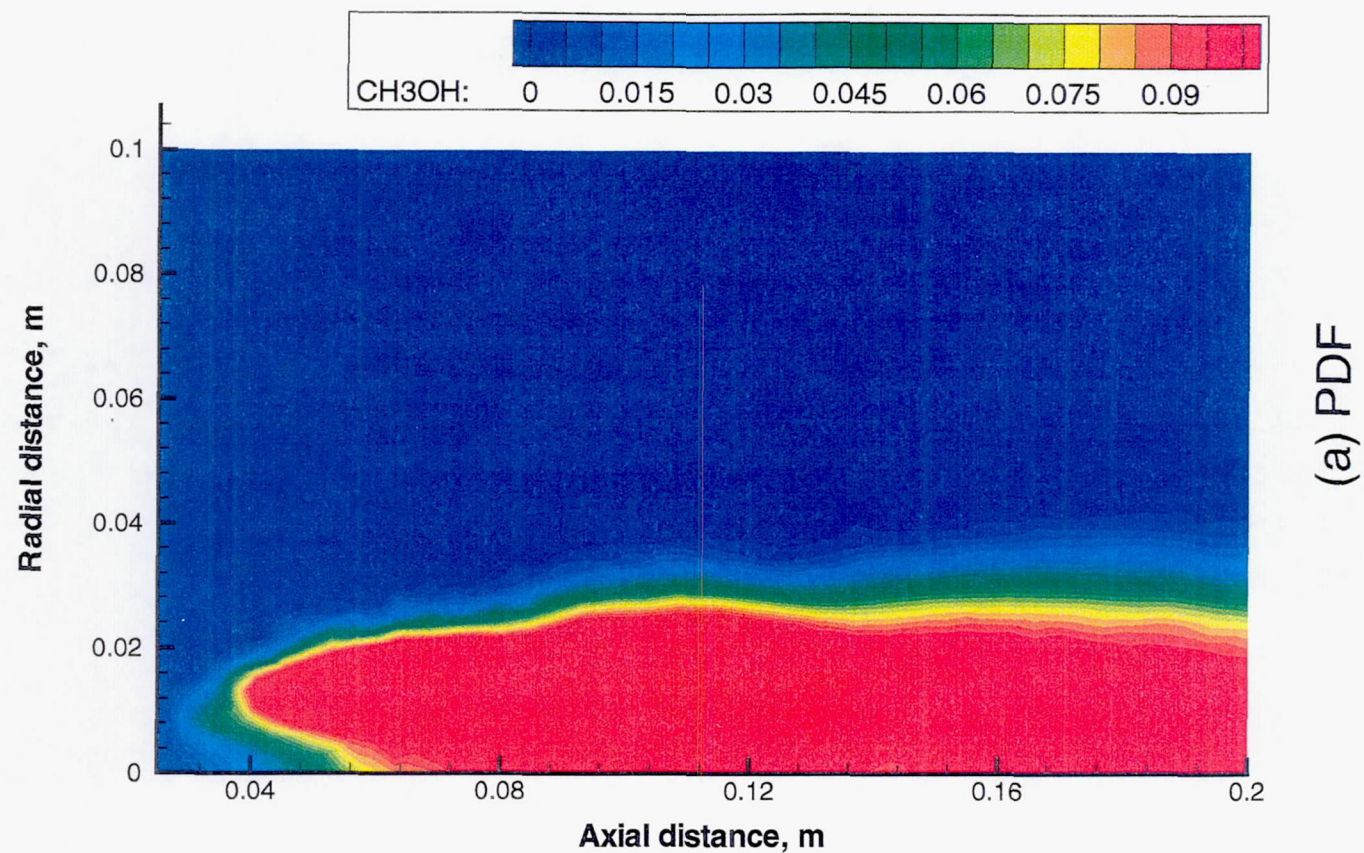mean temperature and velocity and spray droplet locations.
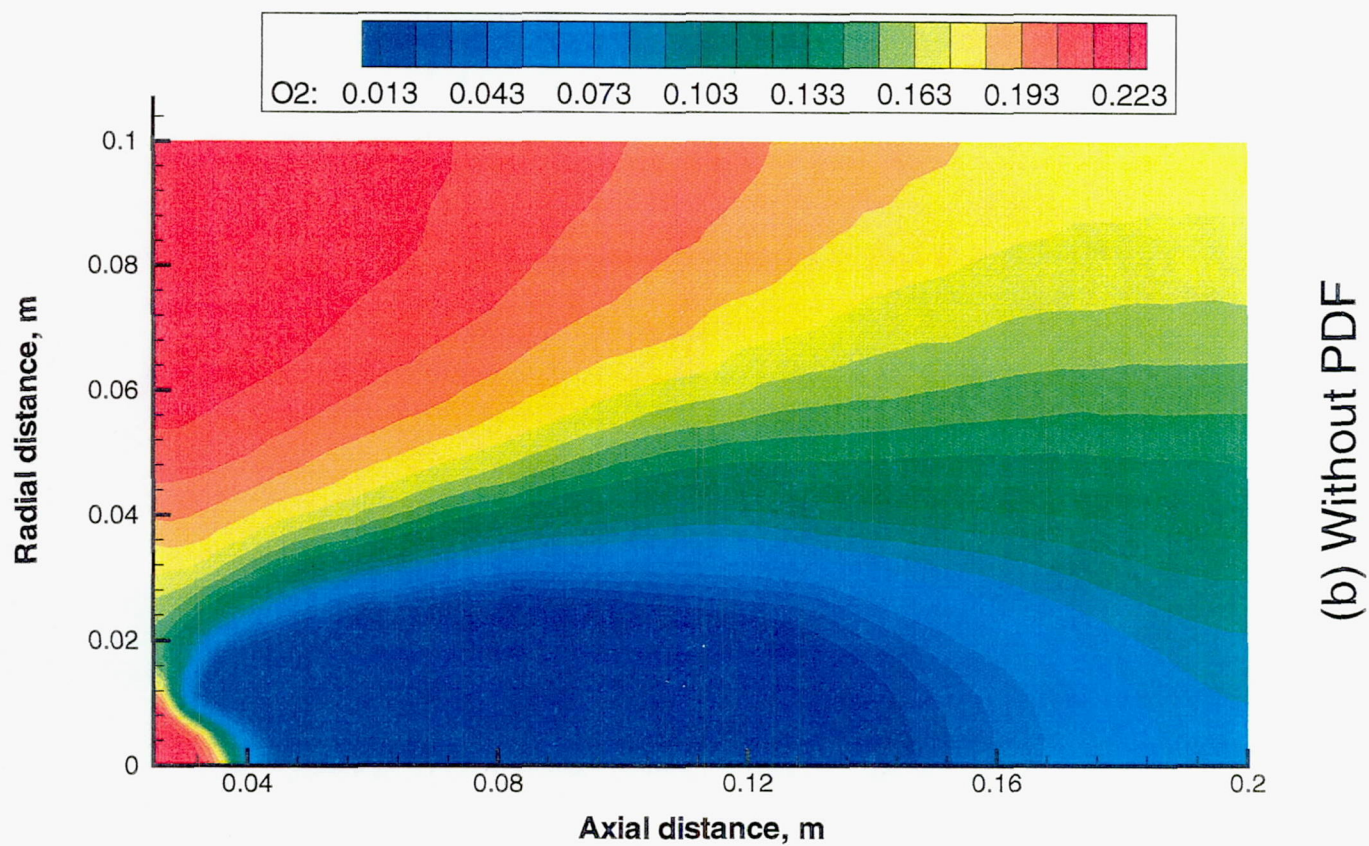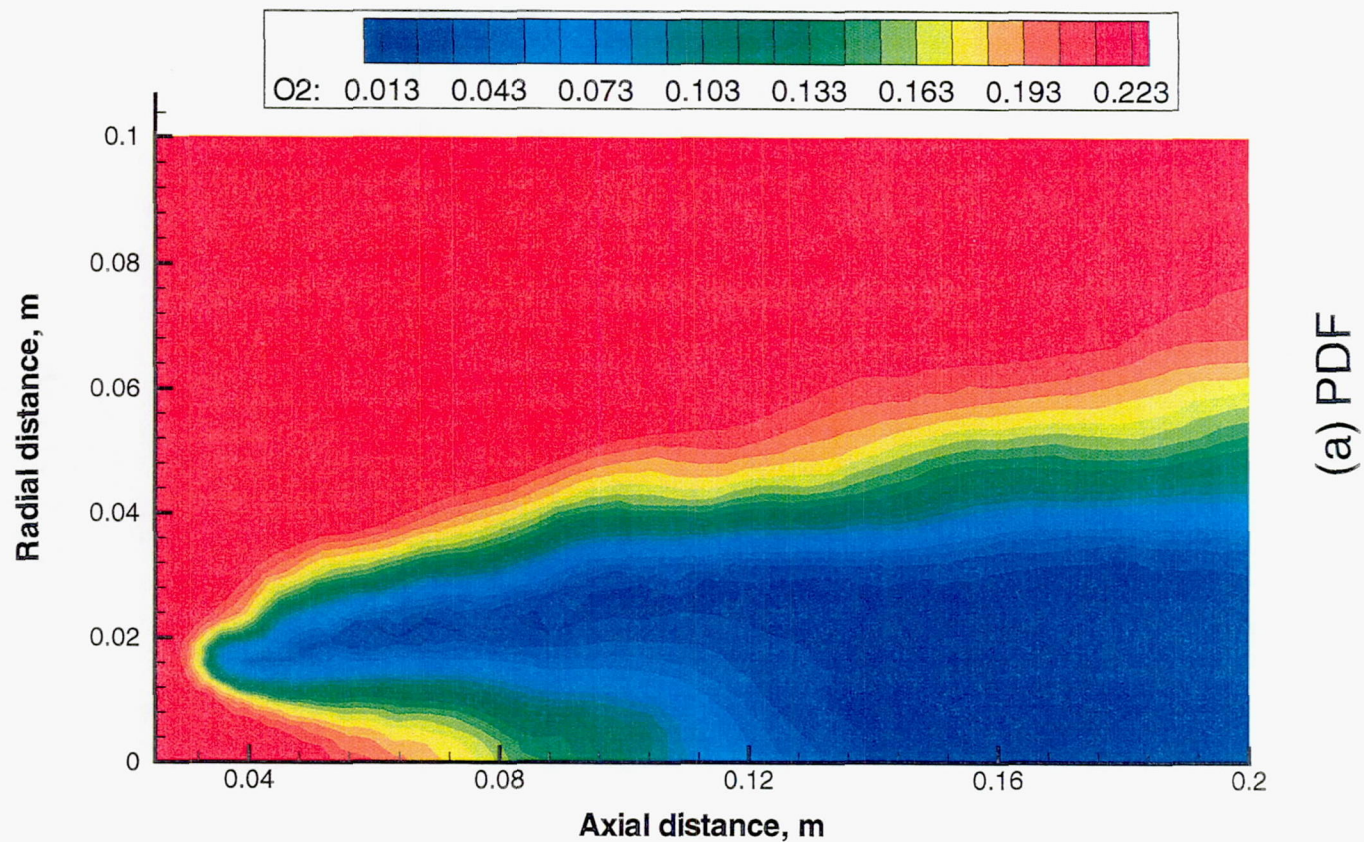
Fig. 5 Gas-phase mean fuel mass fractions contours for Case 1.

O2: 0.013 0.043 0.073 0.103 0.133 0.163 0.193 0.223

Radial distance, m

Axial distance, m

(a) PDF

O2: 0.013 0.043 0.073 0.103 0.133 0.163 0.193 0.223

Radial distance, m

Axial distance, m

(b) Without PDF

Fig. 6 Gas-phase mean oxygen mass fraction contours for Case 1.

6

4.1 A General Description of the McDonell and Samuelsen Cases[8]

The schematic of the experimental facility used at UCI (University of California, Irvine) is shown in Fig. 1. It made use of the RSA (Research Simplex Atomizer) which was manufactured by Parker and Hannifin. The reported methanol and air mass flow rates were 1.26 and 1.32 g/s, respectively. The spray was injected downwards from the center of a 495 x 495 mm square duct and air was pulled through the top of the duct by a blower at a bulk velocity of 0.8 m/s in order to provide adequate entrainment needs. Both the droplet and gas-phase velocities as well as the droplet sizes were measured by making use of a two-component PDI (Phase Doppler Interferometry), and the gas-phase temperatures were measured by using a traversing hot-wire thermocouple. Using the setup shown in Fig. 1, several measurements involving the gas-phase velocity, droplet size and velocity, droplet number flux, and mean gas-phase temperatures were reported at different axial locations starting from 2.5 cm.

The back-lit experimental photographs of the sprays are shown in Fig. 2. In the reacting case, the drops are rapidly consumed downstream of the atomizer. In both cases, droplets at the centerline persist the farthest downstream.[8]

In both the cases, the computations were performed on a 2D axisymmetric grid of 1850 triangular elements as shown in Fig. 3. Since it is not always possible to identify and delineate critical regions of a flow-field in complex 3D geometries, a relatively coarse mesh was chosen to see how well the flow-field could be computed without resorting to a fine grid. The turbulent Schmidt and Prandtl numbers were taken to have a value of 0.70. For the PDF solution, it was obtained by making use of 100 particles per cell. The temperature and species fields supplied to the CFD and liquid-phase solvers were obtained from averaging the PDF solutions over a period of the last 100 time-steps. The calculations were advanced until a steady state solution was reached by making use of the following time steps: Δt_g was determined based on a local time-stepping scheme with a CFL number of 1, $\Delta t_{injection} = 1.0$ ms, and $\Delta t_k = 0.01$ ms. At the end of every liquid-phase injection time step, a new spray distribution comprised of 124 different droplet groups was introduced.

4.1.1 Case 1: A Reacting Spray Case of McDonell and Samuelsen[8]

4.1.1.1 Global Features of the Spray Flame

The global features of the spray flame are shown in Figs. 4a and 4b by presenting a composite view of the droplet locations and the mean gas-phase temperatures and velocity vectors. The filled white circles show the location of the droplets. The droplet sizes range from few microns to 140 microns. The shaded contour lines show the temperature distribution, and the arrows denote the velocity vectors. Fig. 4a shows the results from the PDF method and Fig. 4b shows the results from the non-PDF (conventional CFD) method.

First, let us look at the droplet distribution. As expected, because of the prevailing high temperatures, the droplets in the central region of the spray tend to vaporize faster than those present in the outer regions of the spray. For that reason, the average size of the droplets in the central region is much lower than those present elsewhere. However, most of the droplet mass is contained within the droplets of the high temperature region. The largest droplets found outside of the high-temperation region are sometimes called in the literature as rogue droplets.[8]

Next, let us look at the results from the PDF computations. Combustion seems to be initiated by a flame front stabilized in the lower velocity region of the outer shear layer. Starting from there, the high temperature region spreads in a long v-neck shape as a result of two distinct flames being formed. Methanol is known to vaporize rapidly, its vapor has the same density as air, and its liquid saturation temperature is about 263 K.[8] Early vaporization leads to the formation of a small inner region of premixed fuel with air. Further vaporization downstream leads to a large accumulation of fuel vapor inside of the central high-temperature region (Fig. 5a). This region is also devoid of oxygen (Fig. 6a). Here, combustion takes place with the formation of a diffusion flame where the fuel from the inner central region mixes and burns with the surrounding air from the outer region.

On the other hand, the non-PDF computations in Fig. 4b show that the combustion occurs in a predominantly vaporization-controlled reaction regime. As a result, the high temperature region is spread over a wider region. It lacks a well-defined flame structure that was observed with the PDF computations.

Near the centerline, the PDF results predict higher axial velocities when compared with the non-
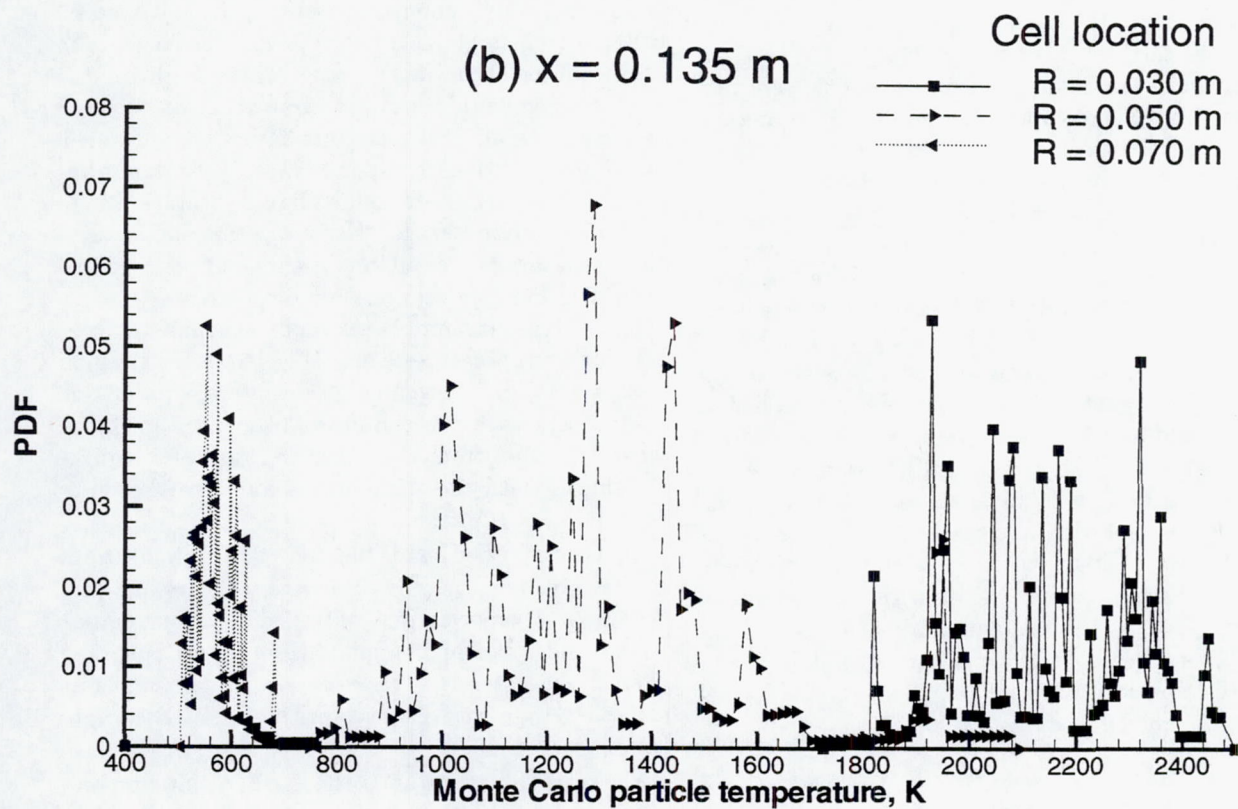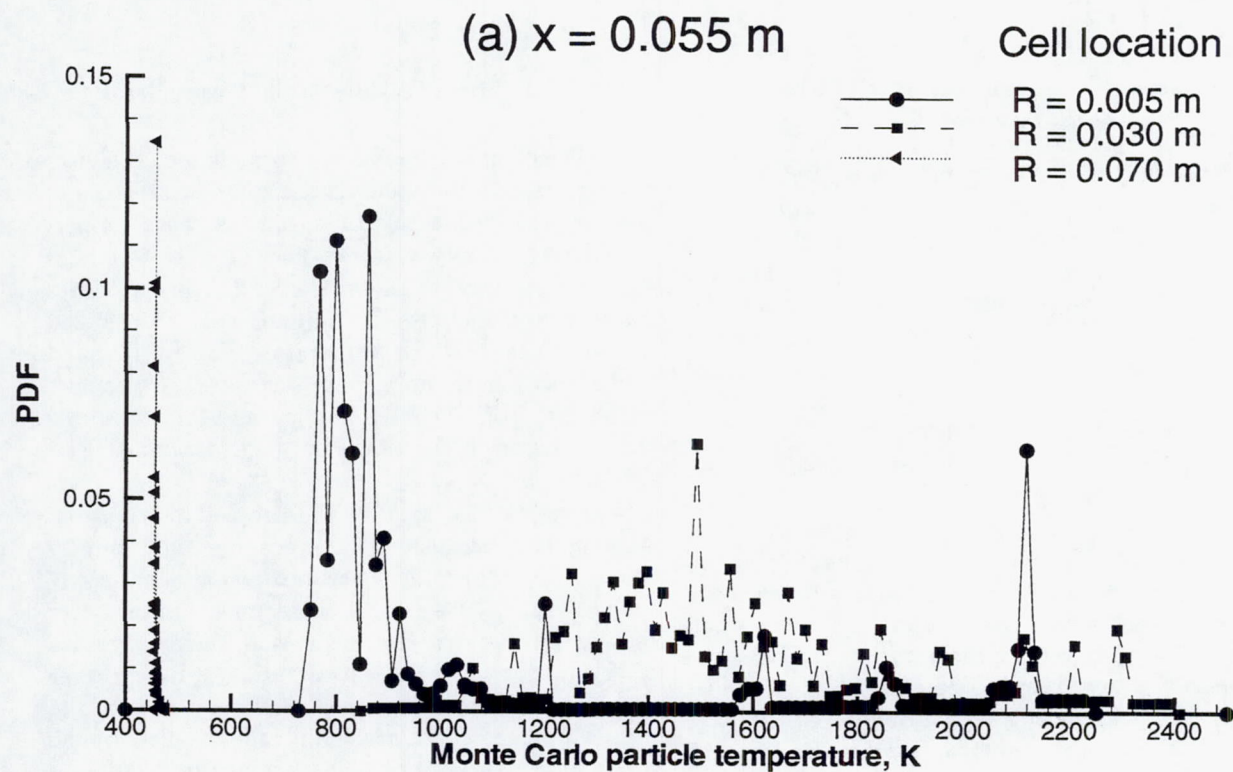
Fig. 7 Gas-phase Monte Carlo particle temperature distribution at three different radial computational-cell locations of Case 1 (Monte Carlo particles/cell =100).
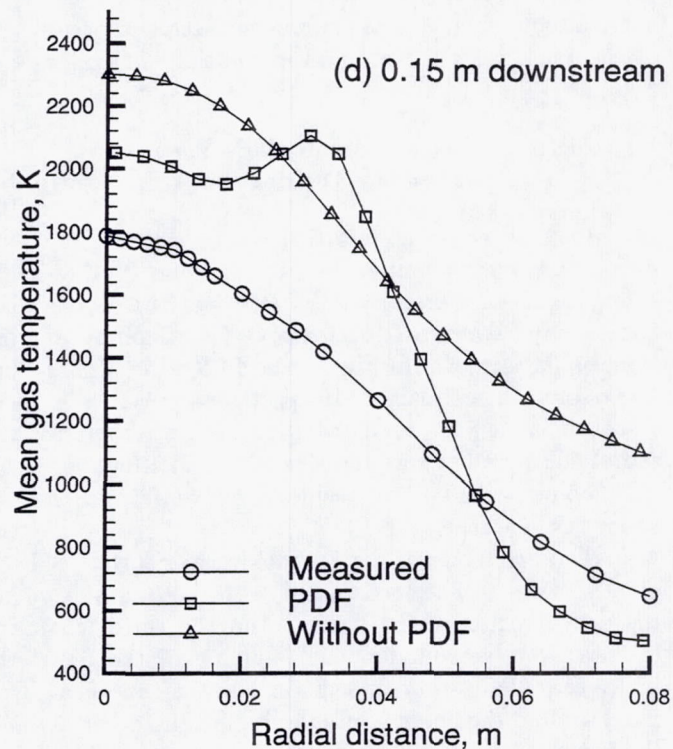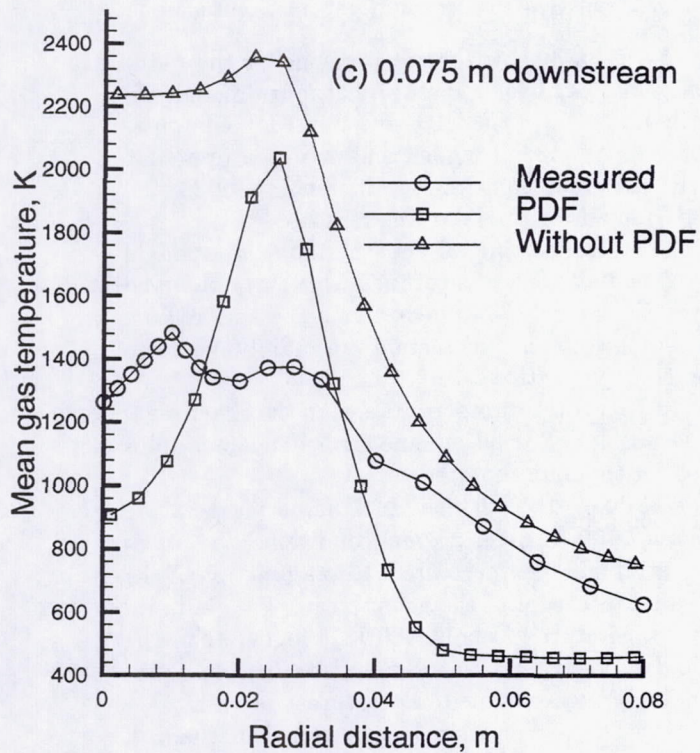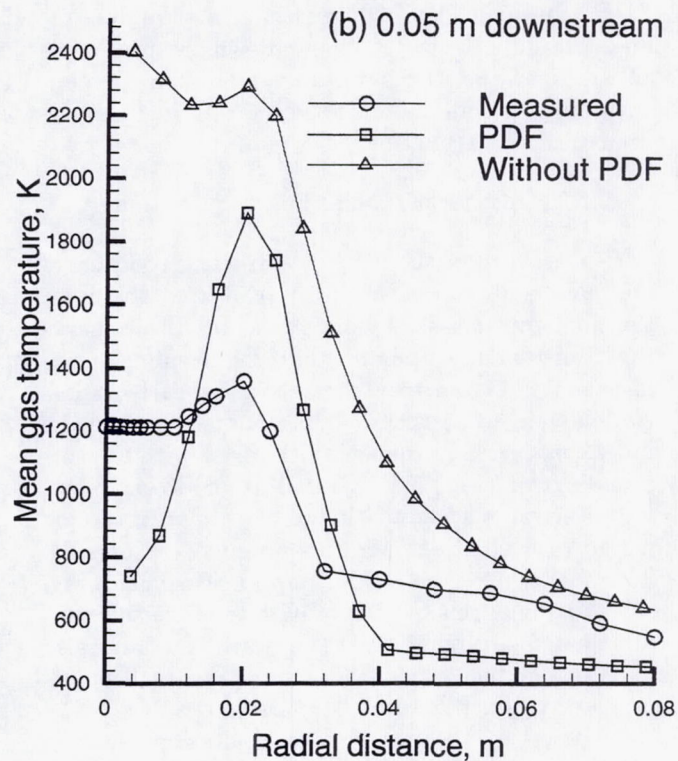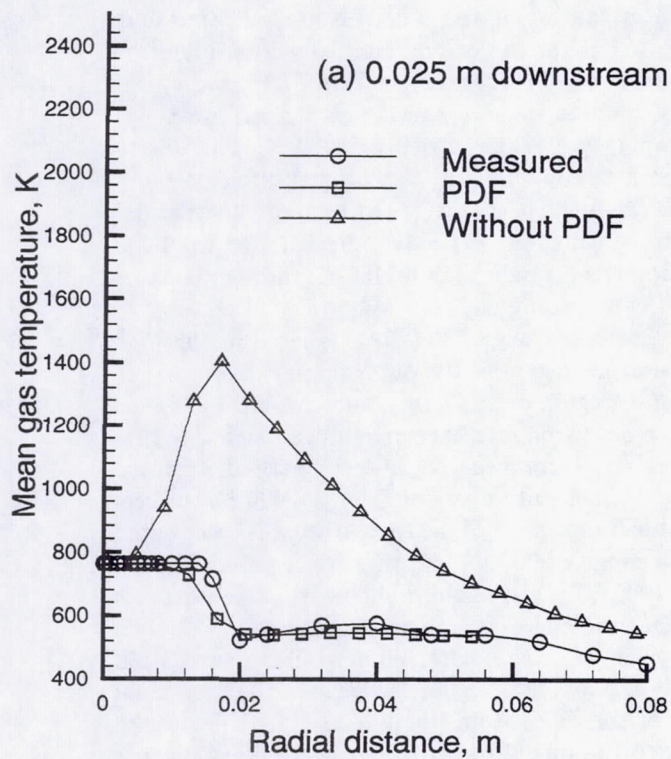
Fig. 8 Gas-phase mean temperature comparisons for Case 1.

PDF solution. The PDF results also show less radial spreading of the jet further downstream. As we sill see later, the PDF results are more in aggrement with the experimental data than those predicted by the non-PDF calculations.

4.1.1.2 Gas-Phase Mass Fraction Contours

Figs. 5 and 6 show the mass fraction contours of methanol and oxygen, respectively. First, looking at the methanol mass fractions reinforces the remarks that were made earlier on the PDF results. Since methanol is known to vaporize rapidly, early vaporization leads to an accumulation of fuel vapor in the inner core region of the jet which mixes with the surrounding air (Fig. 6a). But, further downstream, there is a large accumulation of fuel vapor in the the region where high-temperature products are present. This fuel-rich region is also devoid of oxygen (Fig. 6a). Mixing of this fuel vapor with the outer air supports a diffusion flame. However, this outer flame also feeds on the fuel vapor from the vaporizing droplets present in its active combustion region.

However, the non-PDF computations show a slight accumulation of fuel vapor in only a small region of the entine domain which implies instantaneous burning of the vaporized fuel. Unlike the PDF predictions, the oxygen mass fractions lack a well-defined flame structure as combustion seems to occur over a much wider region in a vaporization-controlled regime.

4.1.1.3 Gas-Phase Monte Carlo Particle Temperature Distribution

In order to examine further what is causing the major differences found in the PDF and non-PDF results, let us take a look at the PDFs of the Monte Carlo temperature distribution of different computational cells as shown in Figs. 7a and 7b. The Monte Carlo solution makes use of 100 particles per cell. Fig. 7a contains the particle distribution at three different radial nodes lying along the side of an axial location at 0.055 m, and Fig. 7b provides similar information at an axial location of 0.135 m.

The first node of Fig 7a falls in the central region of the jet. The second node is located close to the active region of the flame. And the third falls in the outer (surrounding air) region. In the first node, the PDFs show two distinct peaks; one centered around the flame temperature and the other at the temperature of the surrounding reactants. This indicates that some the particles are at flame temperature but the majority are at a lower temperature of the surrounding reactants. The PDF at the next cell is characterized by several peaks distributed over a temperature range of 850 to 2400 K. This distribution is characereristic of a typical diffusion flame where the flame is characterized by large fluctuations in temperature. As expected, the PDF at the third location has a single peak at 450 K, the temperature of the surrounding air.

The first node of Fig 7b is located in the high temperature region of the outer flame, the second in the outer region of this flame, and the third lies even further outwards into the surrounding air. The first PDF is characterized by several peaks distributed over a temperature range of 1800 to 2400 K, the second shows that most of the temperature is distributed over a range of 900 to 1650 K with a remaining few near 1900 K, and the third shows what one expects to see at the edge.

The Monte Carlo temperature distribution clearly shows a substantial variation in the functional form of the PDF from point to point. The results bring to the fore some of the deficiencies associated with the use of assumed-shape PDF methods in spray computations.

4.1.1.4 Mean Gas-Phase Temperature Comparisons

Figs. 8a-d show the comparisons for the radial profiles of mean gas temperature at four different axial locations. Both the PDF and non-PDF computations seem to predict higher peak temperatures than those measured. Some of the differences found could be attributed for the following reasons:

(1) The wetting of the thermocouples might have contributed to some of the uncertainty observed in the the reported temperatures. For this reason, the comparisons in this section are mainly meant to provide a qualitative description.

(2) The uncertainty contained in the experimental data is not clear because no error bands were provided for the data reported.

(3) Even though methanol flame temperature is about 2100 K under normal conditions, the maximum attainable temperature is also a function of the initial temperature of the gas mixture. The bulk inflow temperature of about 450 K is higher than the normal ambient temperature which leads to a correspondingly higher flame temperature.

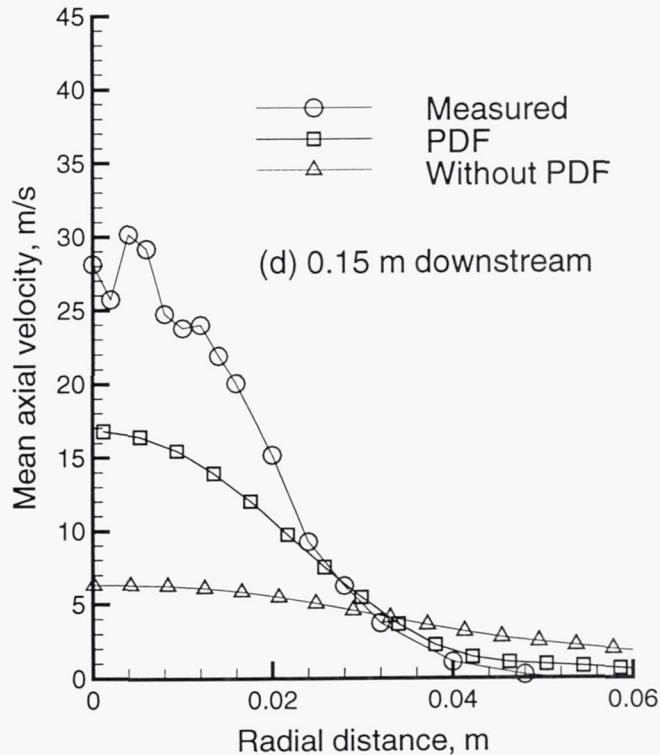(4) The use of a single-step global mechanism is known to overpredict the flame temperatures by
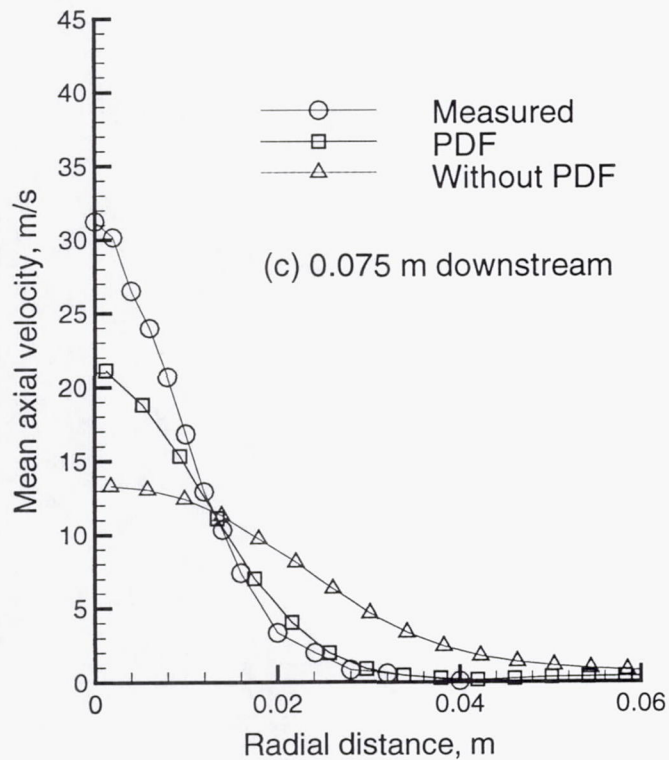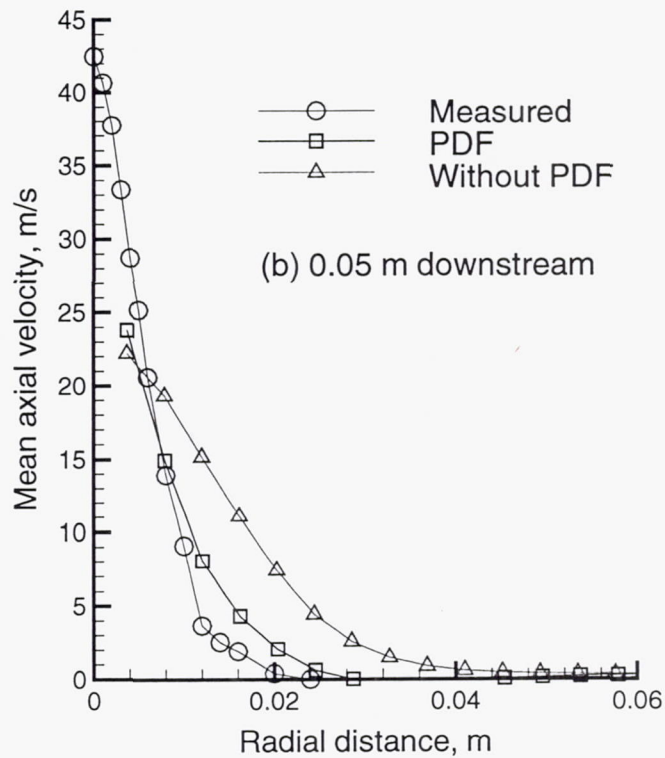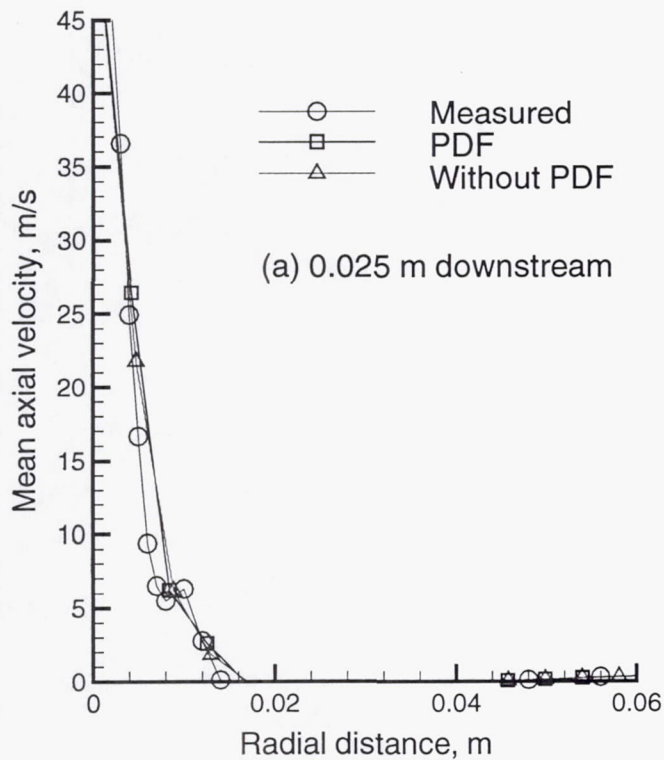
Fig. 9 Gas-phase mean axial velocity comparisons for Case 1.

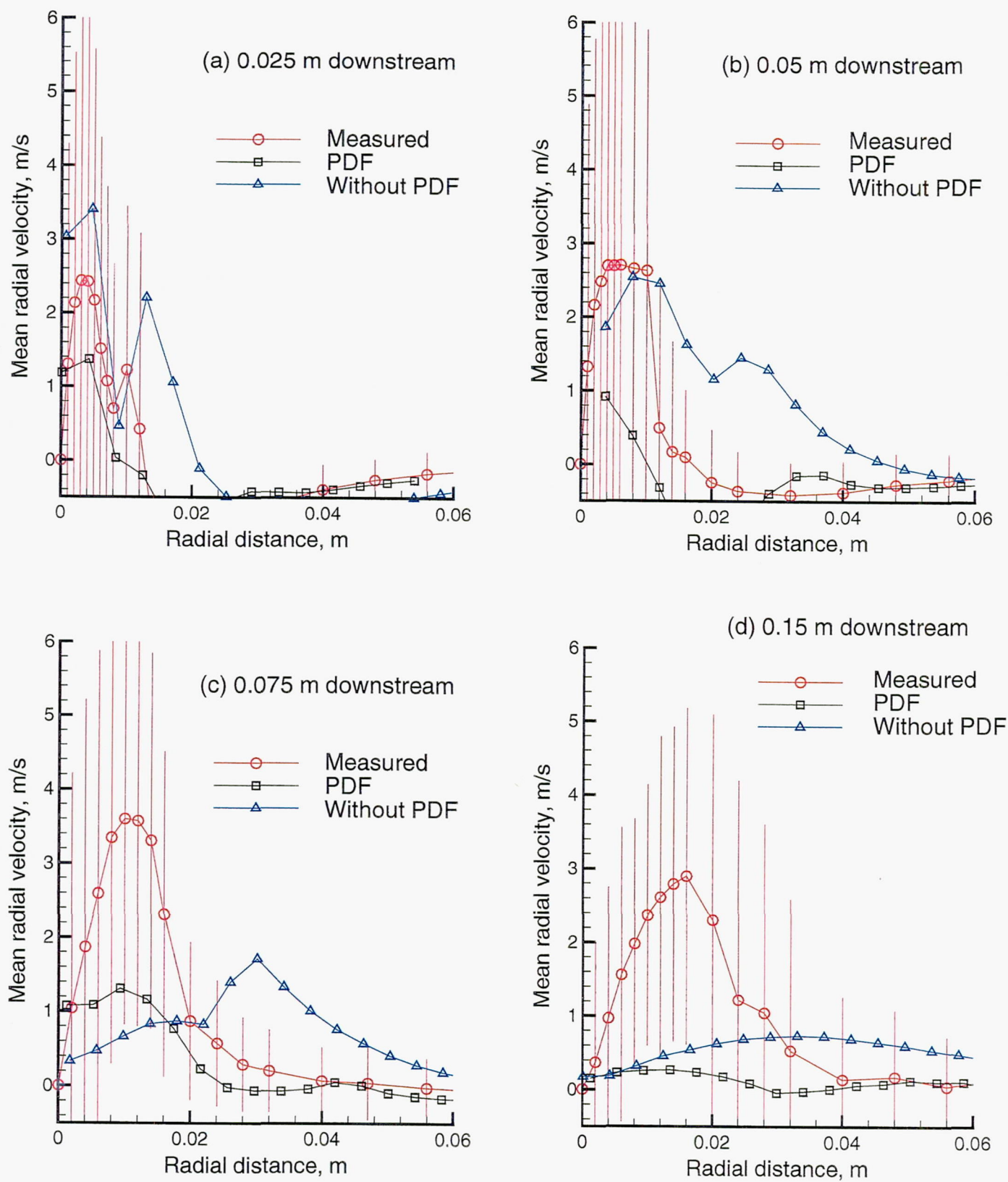Fig. 10 Gas-phase mean radial velocity comparisons for Case 1 (experimental rms is shown as an error bar).
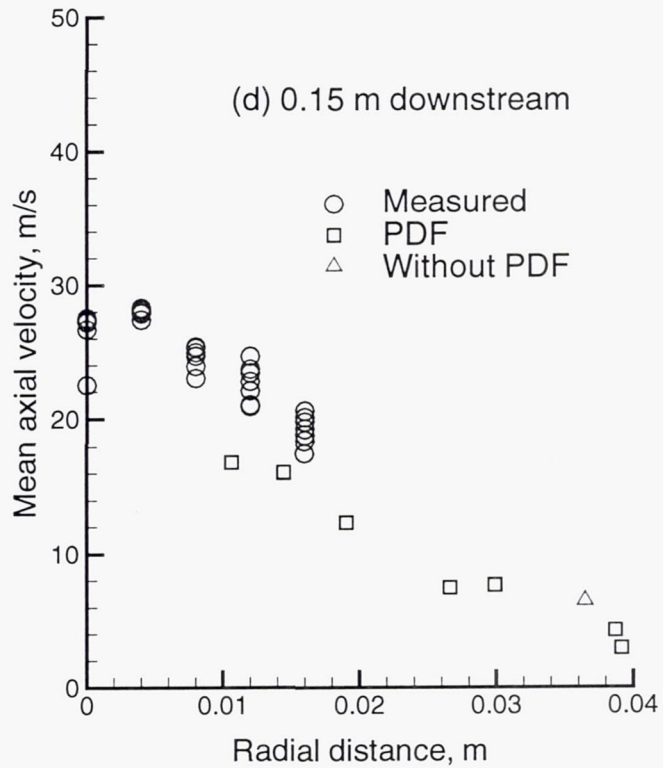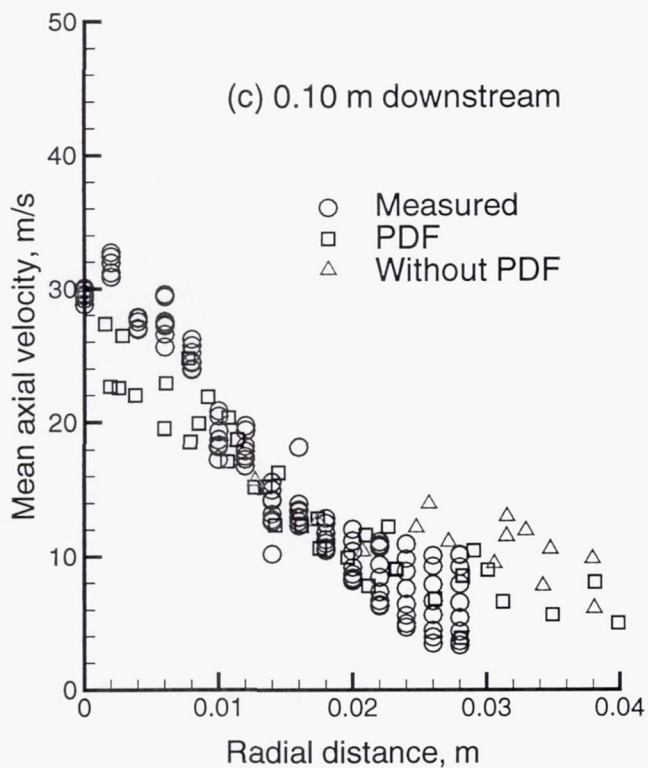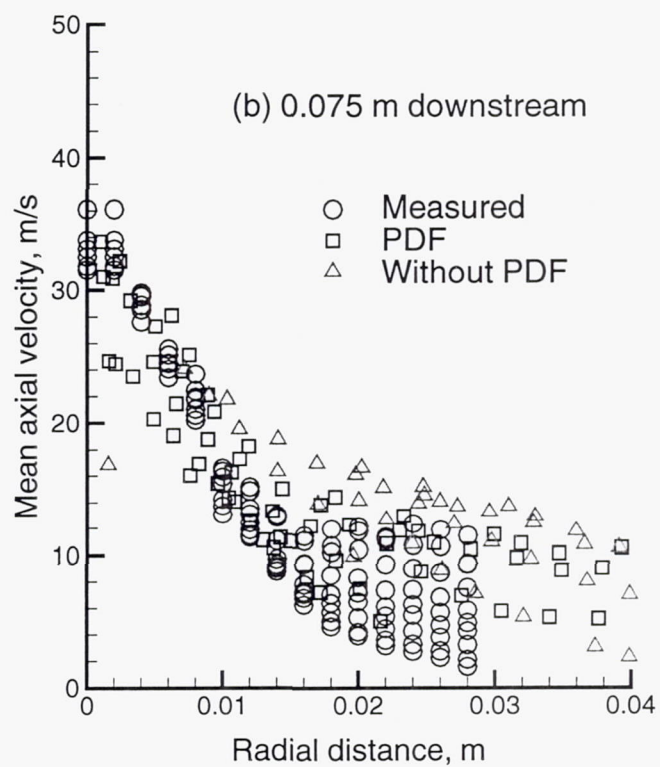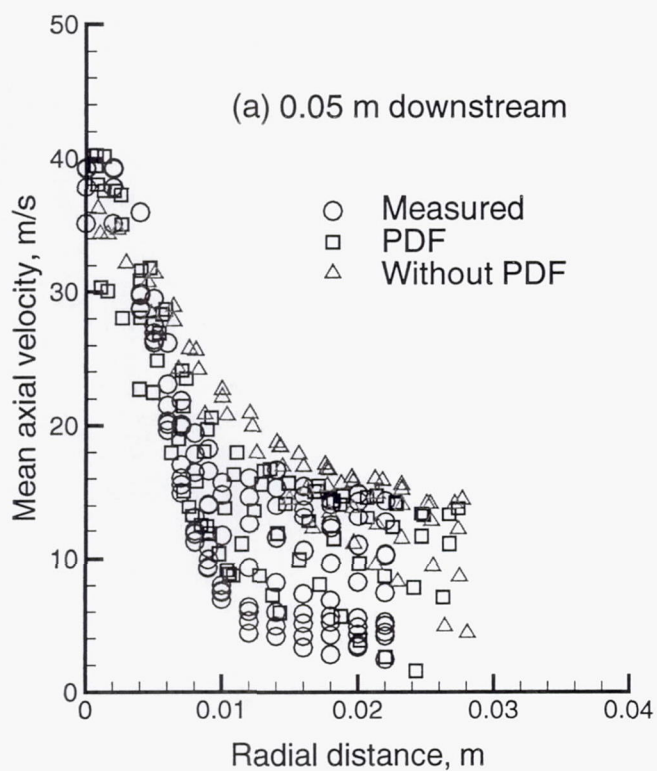
Fig. 11 Drop mean axial velocity comparisons for Case 1.

about 100 to 200 K.

(5) Some of the temperature drop could be attributed to the higher emissivity and radiation cooling rate of the spray combustion flame.

At the inflow in Fig. 8a, if one is wondering why should there exist any differences at all between the measured and computed (both PDF and non-PDF) temperatures, it is because the predictions represent the temperatures extrapolated from those known at the cell centers instead of those specified on the boundary faces of the cells where the inflow conditions were applied. In Fig. 8a, the PDF results show very little change from the specified inflow temperatures, and the results are very close to the specified the experimental data. However, the non-PDF computations show an abrupt jump from the specified inflow temperatures.

At the next location in Fig. 8b, the non-PDF shows the formation of a hot central region with the centerline peak reaching a flame temperature of about 2200 K. Unlike the non-PDF, both the measured and the PDF show the temperature to peak in the outer region of the spray, and the peak temperature location is correctly predicted by the PDF computations. However, the PDF underpredicts the centerline temperature while overpredicting the peak temperature. If you recall from our earlier discussion on the temperature fluctuations in this region, it is quite likely that the measuring devices (thermocouples) may have difficulty in capturing the correct mean temperatures in this region.

At the third location, the PDF again correctly predicts the location of the peak temperature away from the centerline. At the last location, the PDF results predict correctly the shift in the high temperature region towards the centerline. But, in the last two locations, the PDF clearly overpredicts the peak temperatures while also underpredicting the temperatures in the outer regions of the spray. On the other hand, the non-PDF results show a further broadening of the central high-temperature region and a greater radial temperature spreading into the outer region.

4.1.1.5 Gas-Phase Velocity Comparisons

Figs. 9a-d show the comparisons for the mean gas-phase axial velocities at four different axial locations. As expected near the inflow, both the predictions and measurements show similar behavior as shown in Fig. 9a. But at the next three downstream locations of Figs. 9b-d, both the PDF and non-PDF predictions underpredict the velocities near the centerline. The PDF predictions are more closer to what was observed experimentally, and the comparisons become progressively worse further downstream with the non-PDF computations.

The radial velocity comparisons are shown Figs. 10a-d. It is noteworthy that the experimental data seem to show a great deal of turbulent fluctuations when it comes to measuring the radial velocities. For that reason, the rms component of the radial velocity is superimposed as a vertical error bar. The error bars clearly show that the fluctuations are indeed very large and in some instances even exceed the corresponding mean. Similar noise was reported in the data used in our previous comparisons of a swirl-stabilized spray case.[9,10] The PDF correctly predicts the locations of the peaks at all four locations but seem to underpredict the magnitudes by a considerable measure. However, the non-PDF computations tend to overpredict the radial distances of the peak, and the comparisons become progressively worse further downstream. Further improvements in the comparisons might be possible by refining the grid in the jet region.

4.1.1.6 Droplet Velocity & Size Comparisons

The scatter plots of the mean droplet axial velocity are presented in Figs. 11a-d at four different axial locations. These plots include all of the reported measured velocities as well as the Lagrangian droplet velocities. It is noteworthy that the reported measurements of McDonell and Samuelsen[8] don't cover the entire range spanned by the predictions.

The PDF provides a better agreement than the non-PDF, and the non-PDF comparisons become progressively worse further downstream. These comparisons are consistent with the mean gas-phase velocity comparisons discussed earlier. The differences observed near the centerline with the PDF predictions could partially be attributed to the corresponding behavior observed earlier in the gas-phase velocities. As we have discussed earlier, the droplet sizes as predicted by the non-PDF in the central region of the jet tend to be smaller than those measured. This is because the droplets in that region tend to vaporise faster as a result of the higher gas temperatures predicted by the non-PDF (see Figs. 8a-d). This would in turn cause the droplets to relax toward the surrounding gas-phase velocities much faster because of the drag forces acting on the smaller droplets.
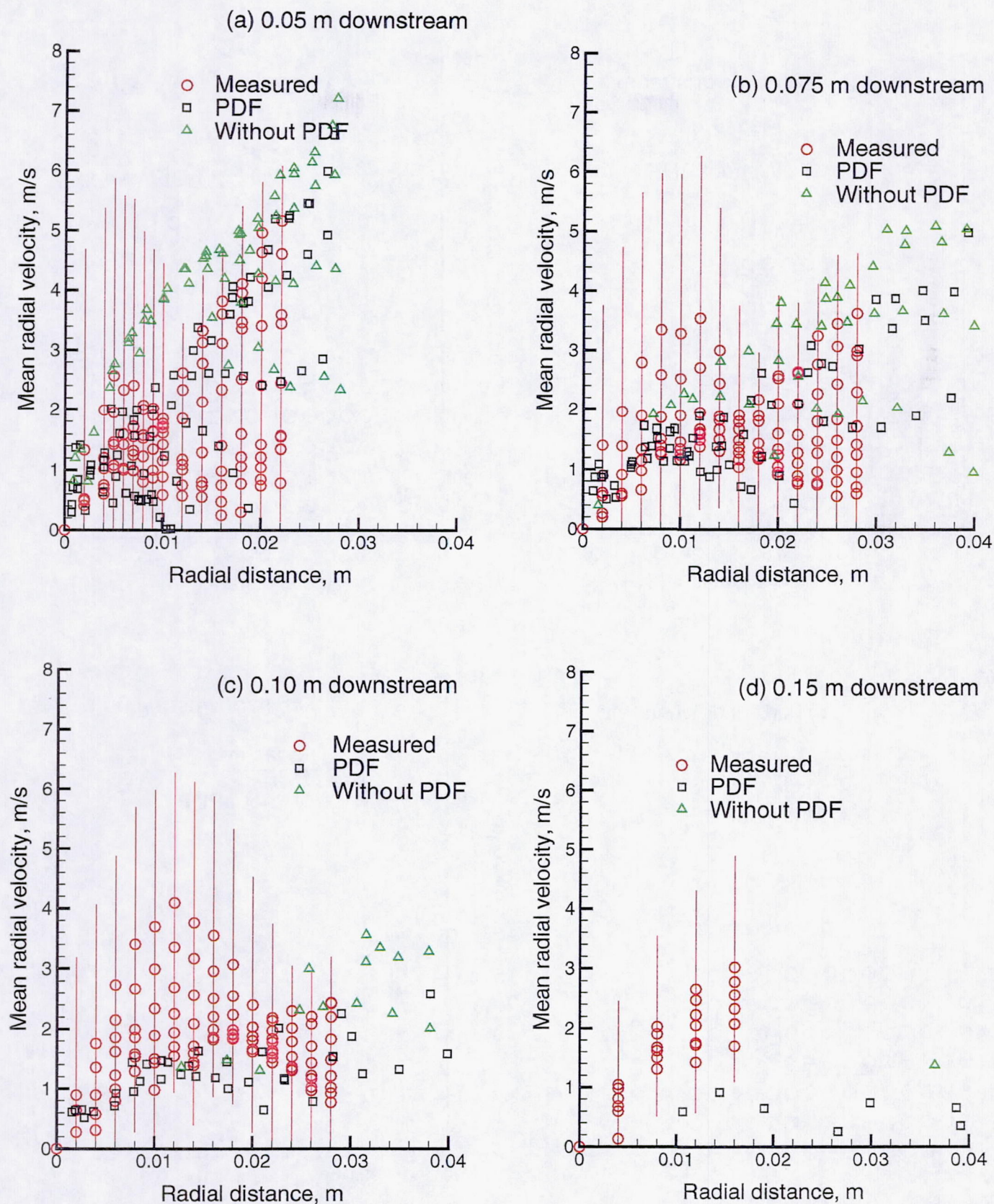
14

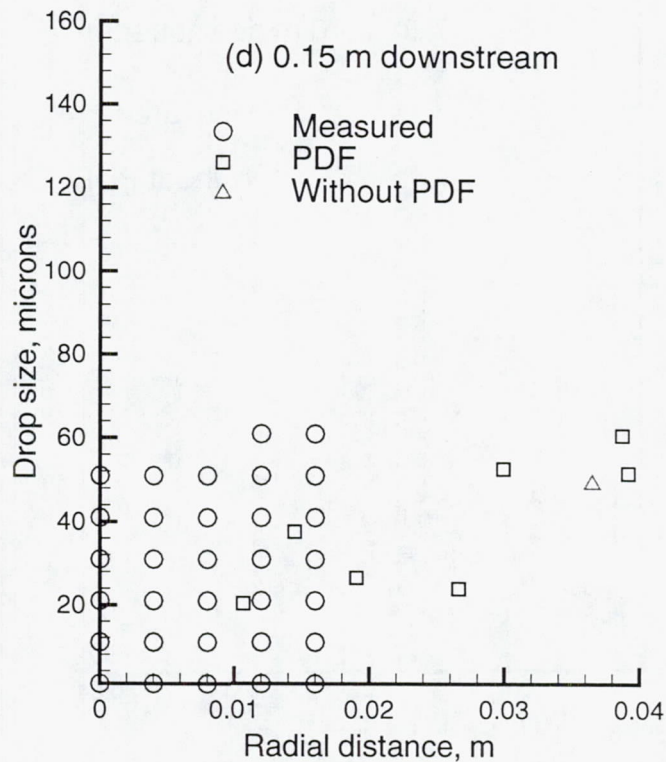Fig. 12 Drop mean radial velocity comparions for Case 1 (experimental rms is shown as an error bar).
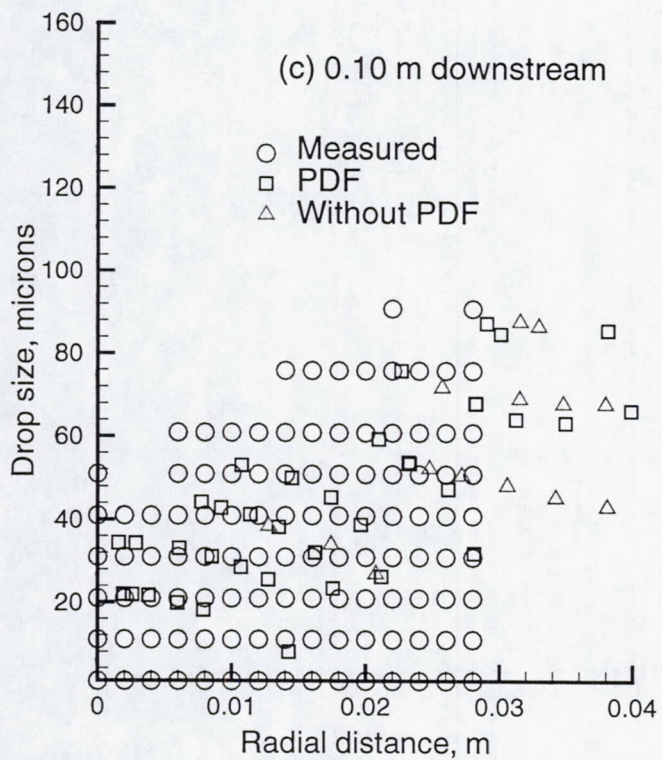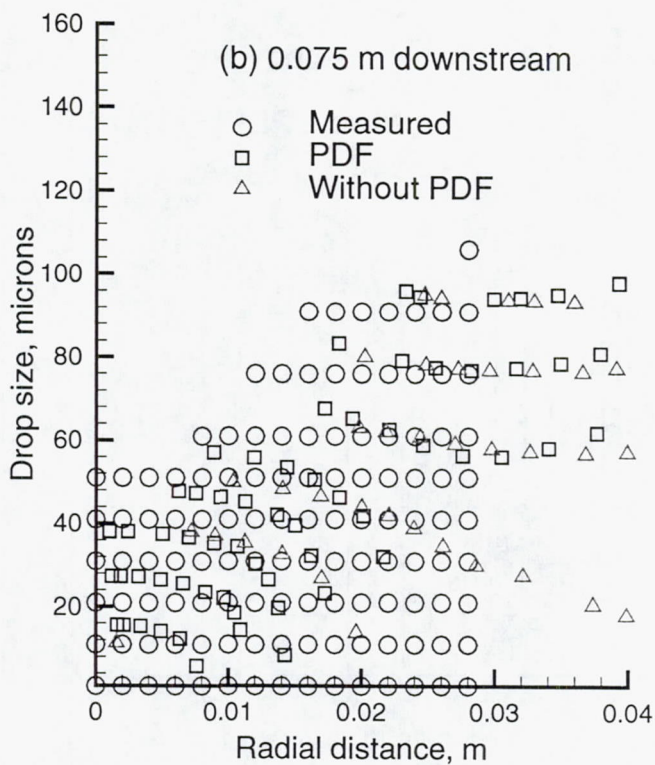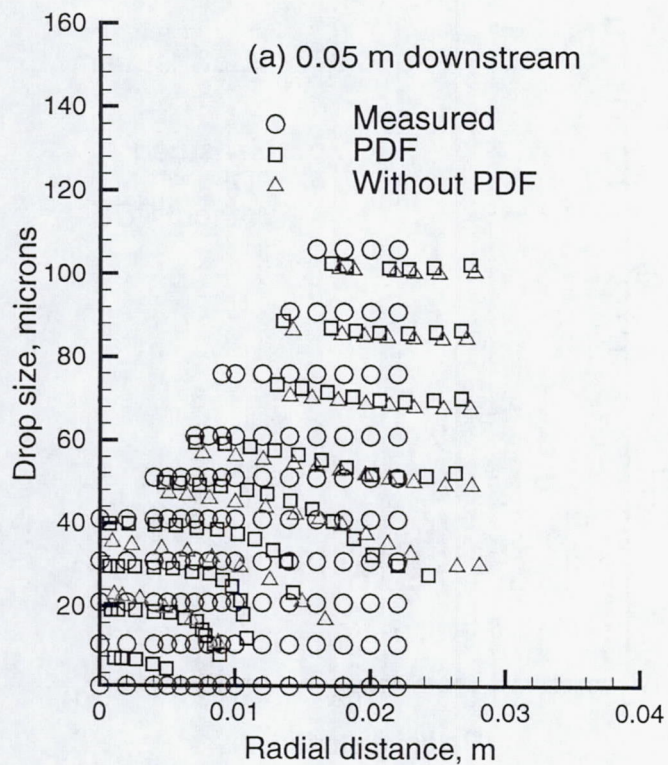
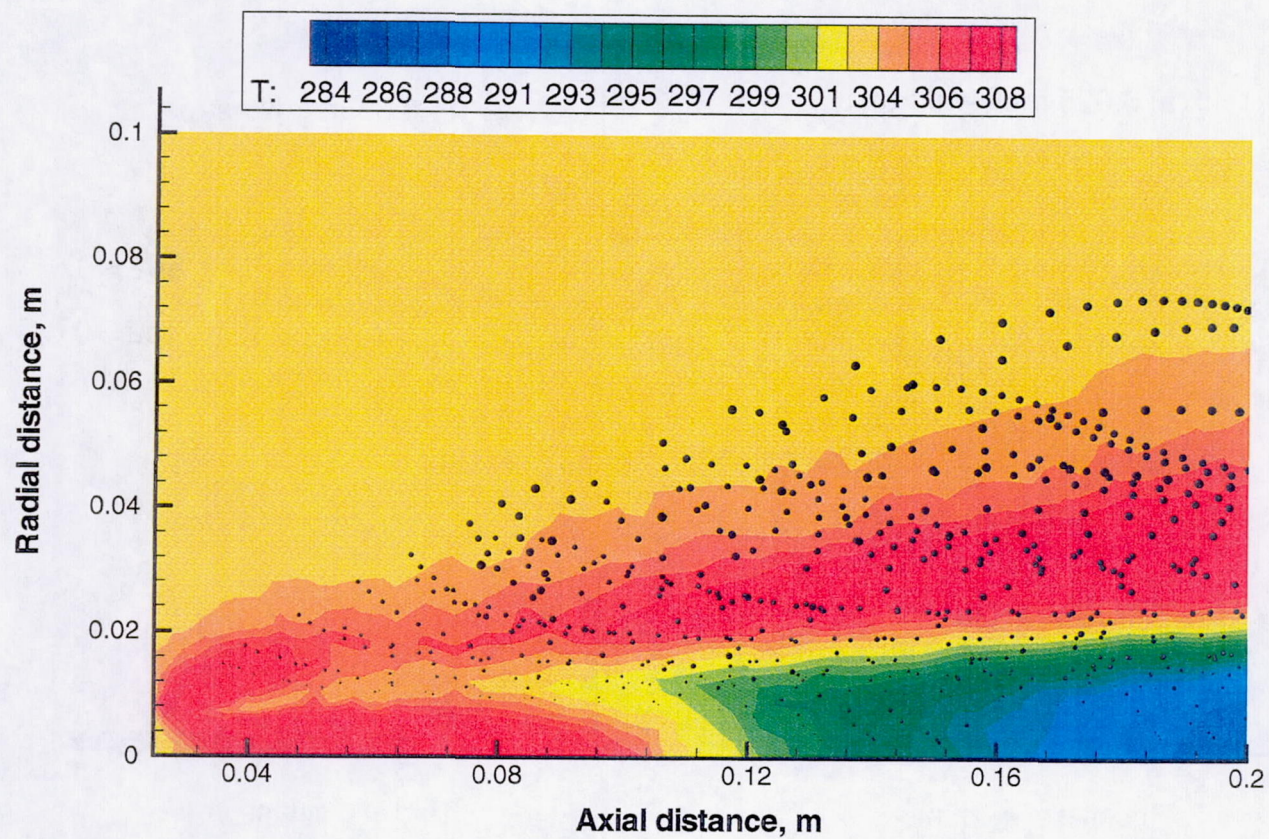Fig. 13 Scatter plot of drop size comparisons for Case 1.

Fig. 14 The global features of a non-reacting spray for Case 2 showing
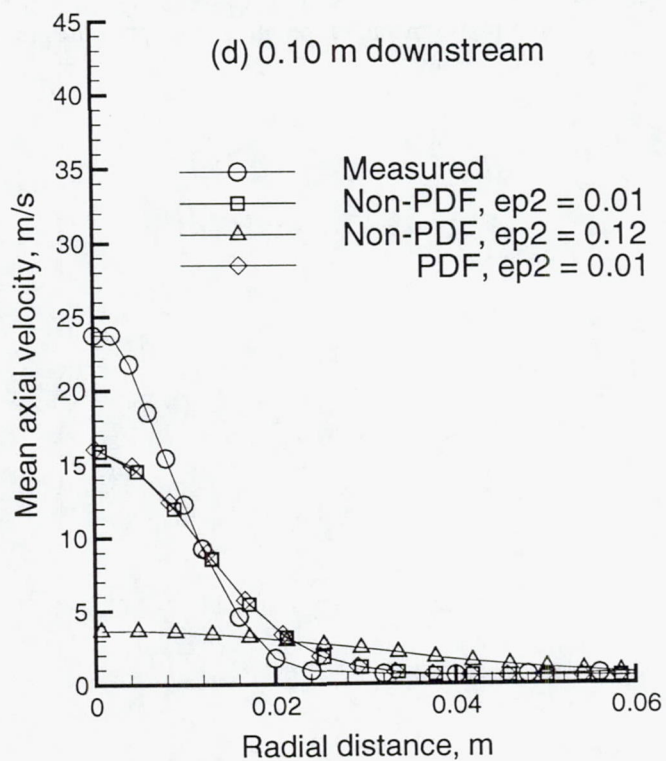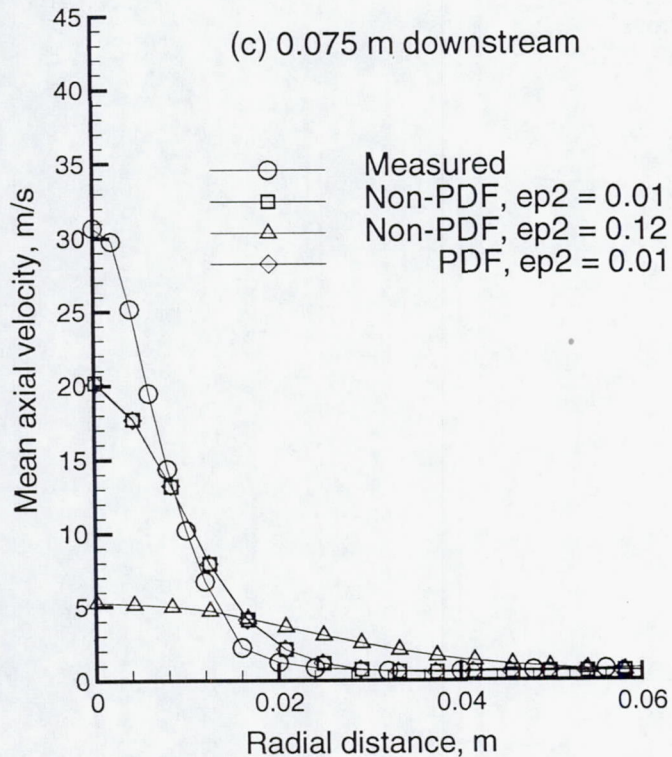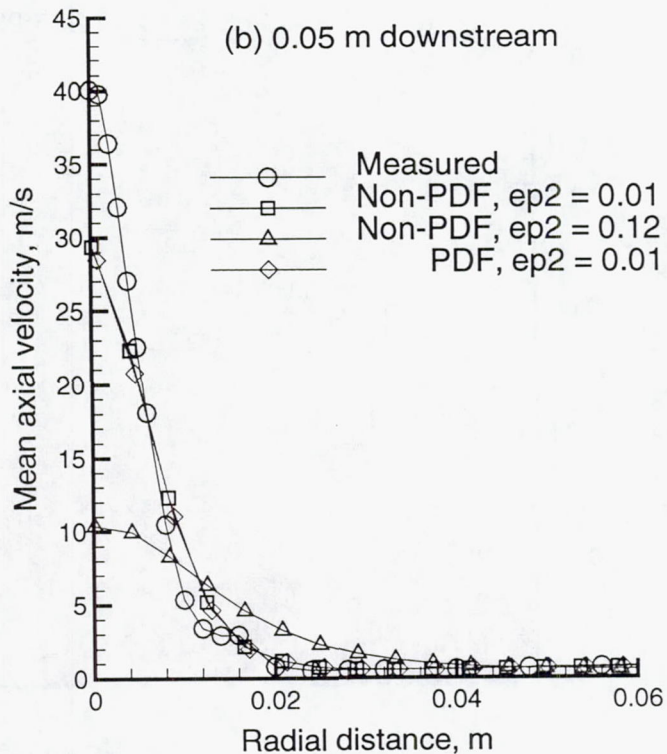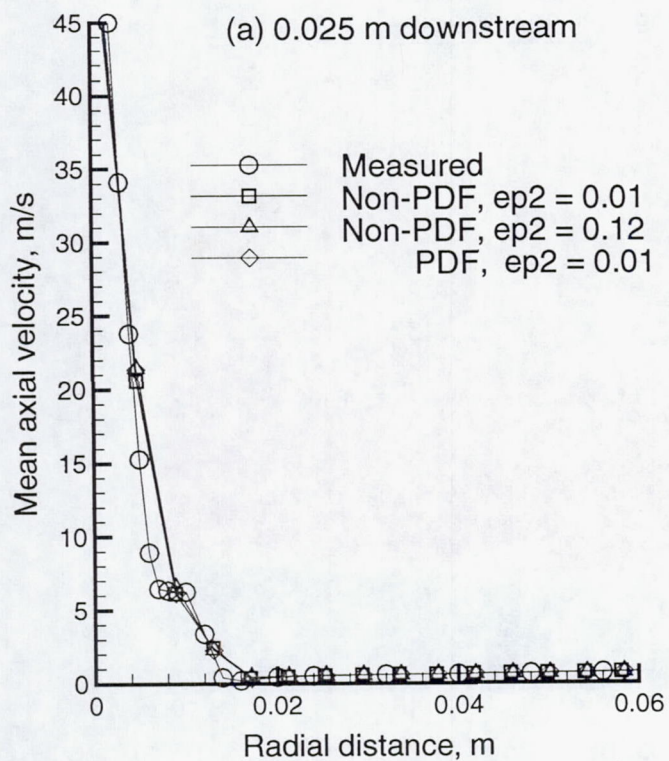gas-phase mean temperature and spray droplet locations.
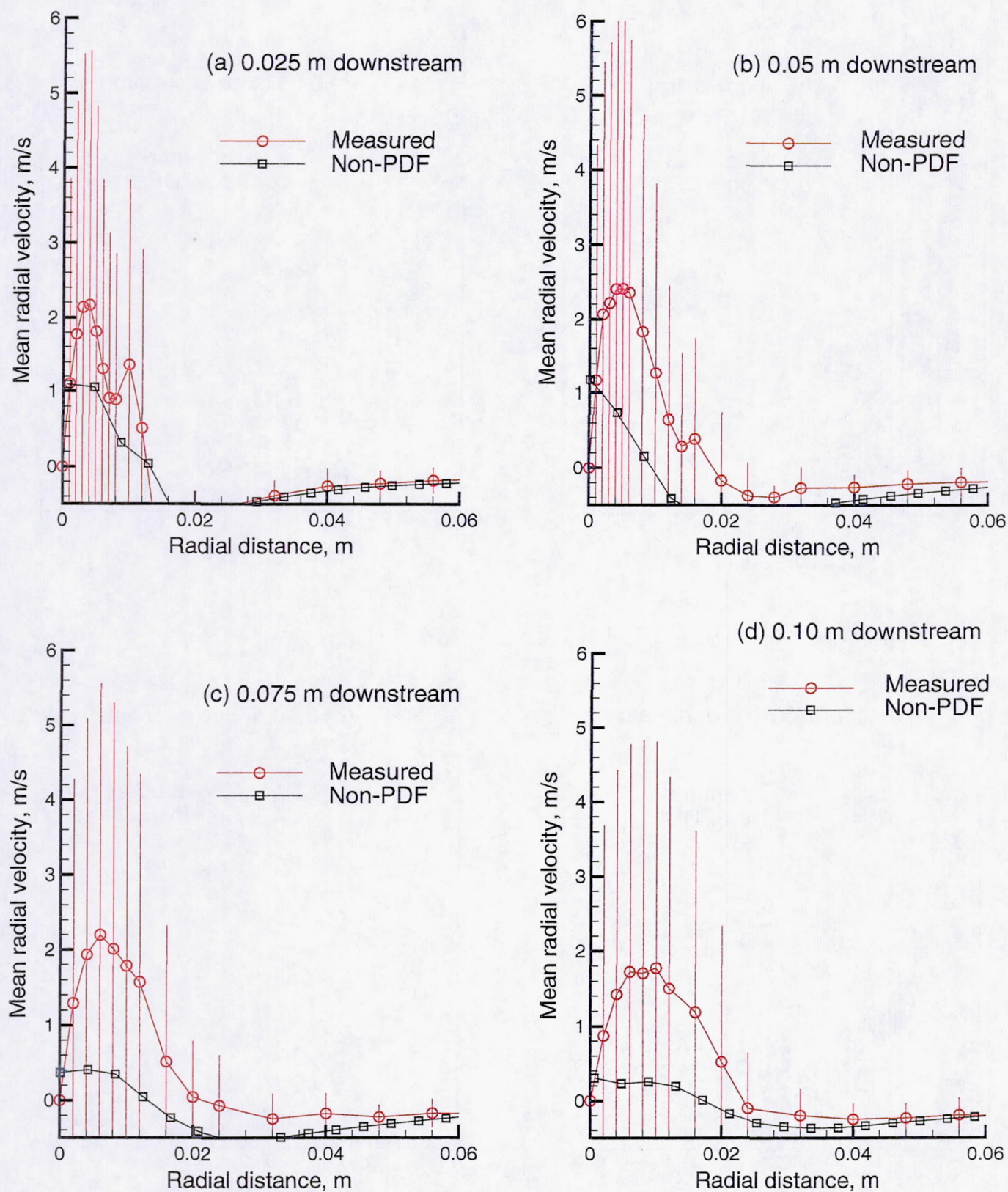
Fig. 15 Gas-phase mean axial velocity comparisons for Case 2.

Fig. 16 Gas-phase mean radial velocity comparisons for Case 2 (experimental rms is shown as an error bar).
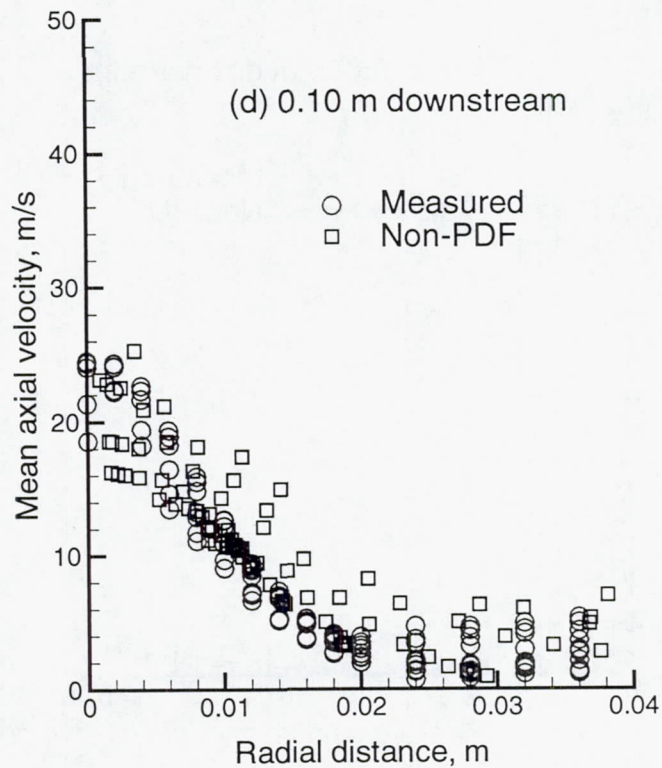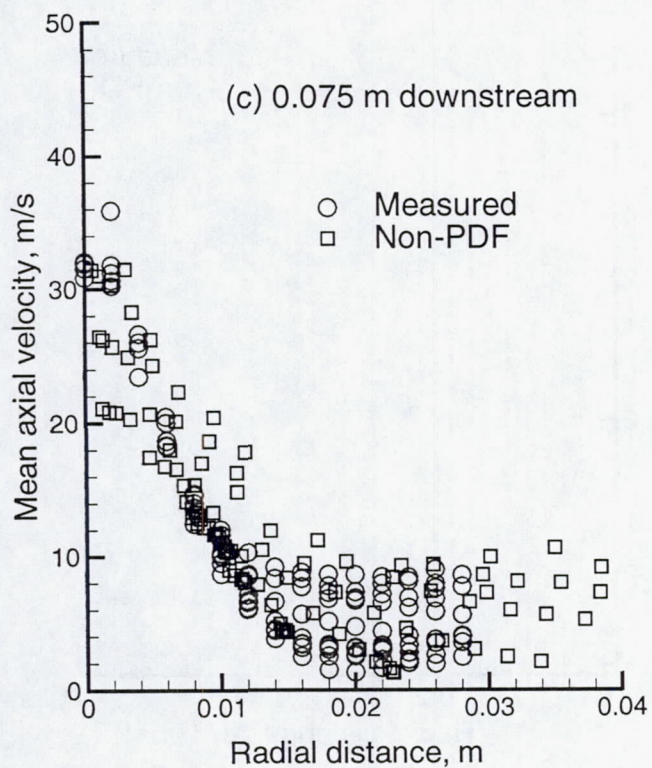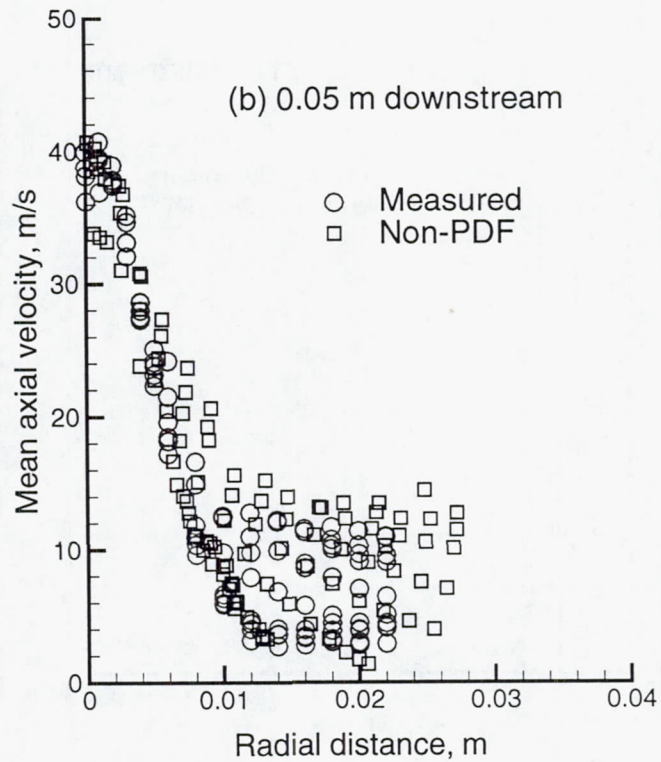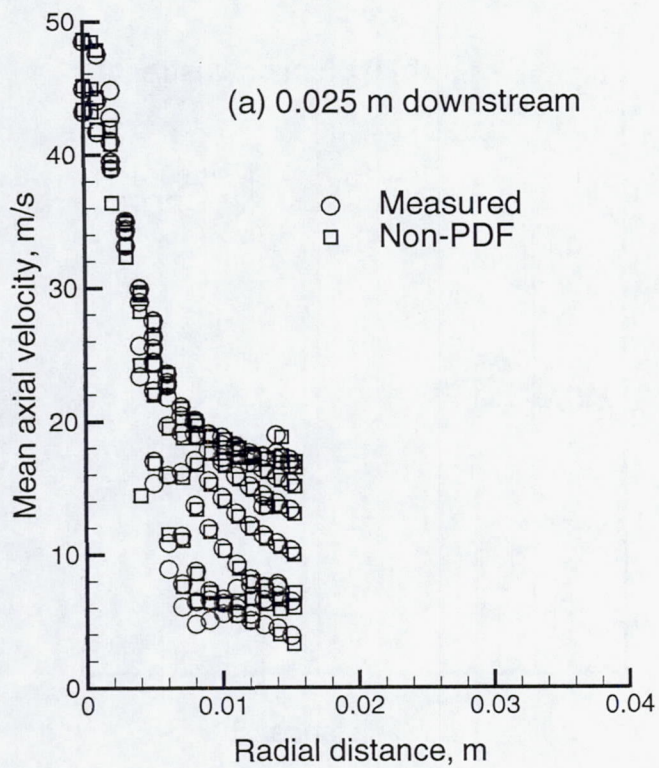
Fig. 17 Drop mean axial velocity comparisons for Case 2.

Figs. 12a-d show the scatter plots of mean droplet radial velocity. As in the gas-phase, the experimental data show a great deal of turbulence when it comes to measuring the radial velocities. The error bars based on the rms component clearly show that the fluctuations are very large and in some instances even exceed their corresponding mean. Both the PDF and non-PDF comparisons underpredict the experimental data. The PDF computations are able to capture the qualitative trends correctly but the non-PDF comparisons become progressively worse further downstream.

Fig. 13a-d show the scatter plots of droplet sizes. The experimental data is reported in the form of several radial measurements for a given droplet-size range. Unfortunately, the plots do not contain any information on the number density of a given droplet group. Although the experimental data shows a wider presence radially, only some of the droplet groups do contain most of of the mass. The results show that the droplet sizes are well represented by both the PDF and non-PDF computations but the non-PDF computations show a far less number of droplets within the reported experimental range of the last location. In the non-PDF computations, the droplets traversing the central region of the jet vaporize more rapidly as they are exposed to temperatures of about 2100 K for a longer period of time. This would explain the reason for the lack of enough number droplets in this range.

4.1.2 Case 2: A Non-Reacting Spray Case of McDonell and Samuelsen[8]

4.1.2.1 Global Features of the Flow-field

The global features of the flow are shown in Fig. 14. Fig. 14 shows the results from the non-PDF method. The results from the PDF solution are not shown as they look similar.

First, let us first look at the droplet distribution. When compared to the reacting case, a lot more droplets are present in the computational domain as only few of the smaller droplets are taken out of computation due to complete evaporation. As a result, most of the droplets leave the domain through its exit boundary. The droplet sizes range from few microns to 140 microns.

The gas temperature distribution ranges between 284 to 308 K. The assigned temperature for the initial droplet internal temperature is 314 K and it is 303 K for the initial gas temperature. For that

reason, the gas temperature rises in the initial stages of the evaporation. The evidence of this effect can be clearly seen in the initial stages of the inner jet and also downstream in the outer regions of the jet. However, further downstream of the inner region, the gas temperature falls as more heat is transferred out of the surrounding gas to support further evaporation of the liquid fuel.

4.1.2.2 Gas-Phase Velocity Comparisons

Figs. 15a-d show the comparisons for the mean gas-phase axial velocities at four different axial locations. The comparisons were made not only to show the differences between PDF and non-PDF computations but also to show the differences in the results obtained from the use of different values used for the parameter, ep2. Ep2 is one of the constants used in controlling the the amount of artificial dissipation added to the CFD computations in the form a Jameson dissipation operator. Further details on this subject can be found in Ref. 11. A value of 0.01 for ep2 represents about the minimum value which is needed to stabilize the computations.

As expected near the inflow, both the predictions and measurements show similar behavior as shown in Fig. 15a. But at the next three downstream locations of Figs. 15b-d, the predictions underpredict the velocities near the centerline. For this non-reacting case, both the PDF and non-PDF predictions produced identical results. The effect of increasing the artificial viscosity can clearly be seen as increasing the value of ep2 from 0.01 to 0.12 causes considerable degradation in the predictions. Further improvements in the comparisons might be possible by refining the grid in the jet region.

The radial velocity comparisons are shown in Figs. 16a-d. The computations starting from now and onwards are only reported for the non-PDF case with ep2 = 0.01 as both the PDF and non-PDF predictions produced very similar results. The comparisons for radial velocities are similar to what was reported for the reacting case.

4.1.2.3 Droplet Velocity & Size Comparisons

The scatter plots of the mean droplet axial velocity are presented in Figs. 17a-d at four different axial locations. These plots include all of the reported measured velocities as well as the Lagrangian droplet velocities. It is noteworthy that the reported measurements of McDonell and Samuelsen[8] don't cover
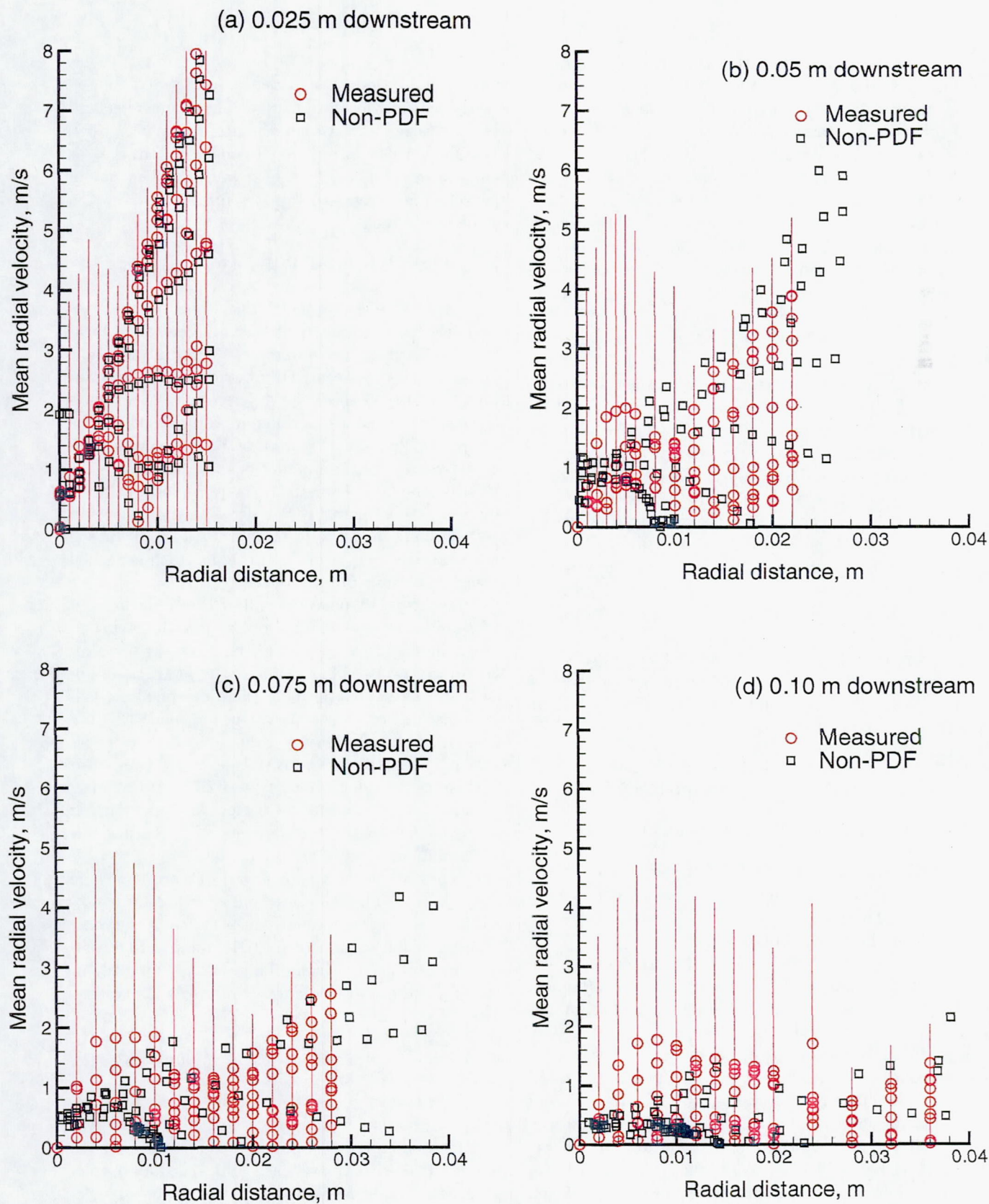
Fig. 18 Drop mean radial velocity comparions for Case 2 (experimental rms is shown as an error bar).
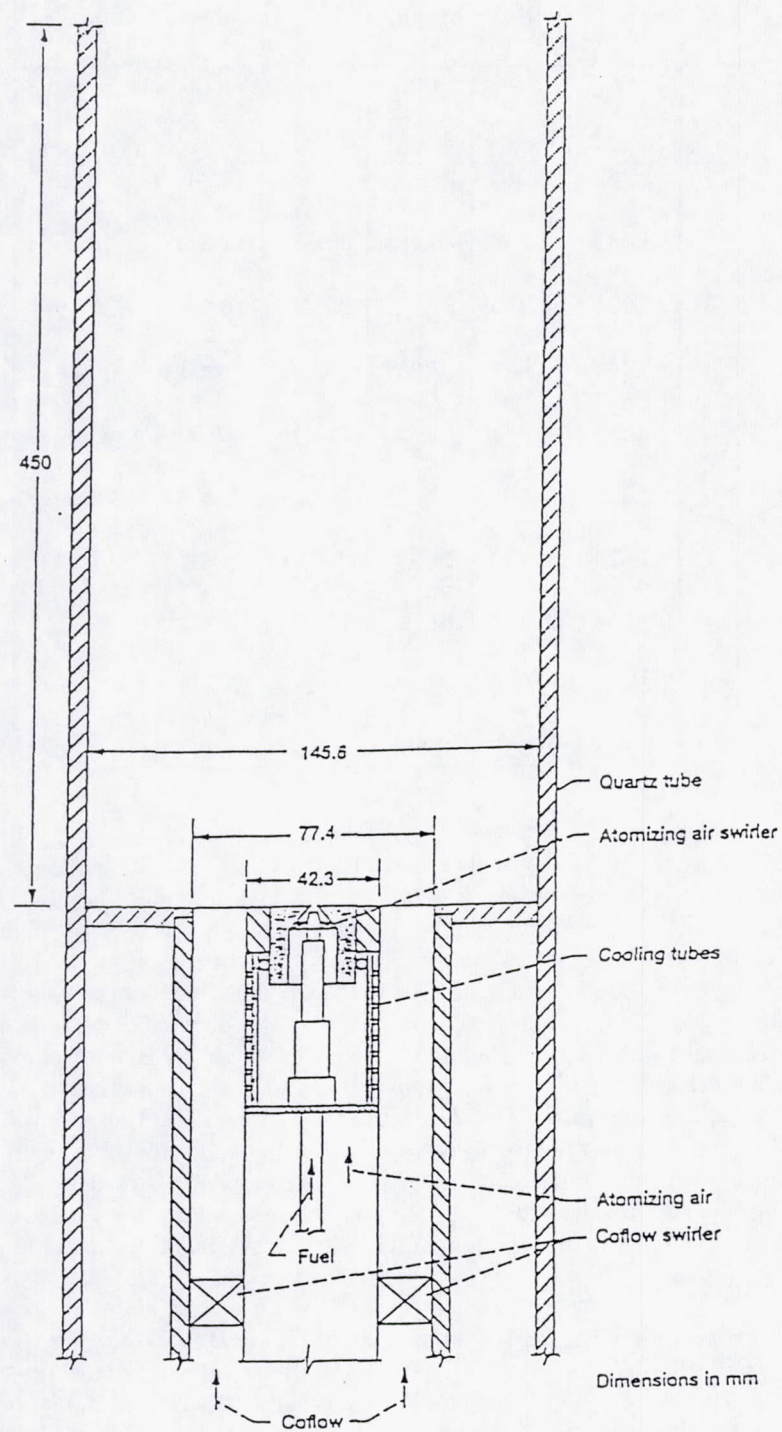
Fig. 19   Schematic of the confined swirl-stabilized,
n-heptane, spray-flame burner for Case 3.

Table 1. Swirling spray initial conditions for Case 3.

k	m_{ko} (mg/s)	r_{ko} (mm)	u_{ko} (m/s)	v_{ko} (m/s)	w_{ko} (m/s)	D_{ko} (microns)
1	0.762	6.093	28.159	34.446	15.246	8.62
2	3.031	5.949	25.188	30.130	12.511	19.20
3	4.020	5.215	21.070	22.646	10.227	29.79
4	3.440	4.474	17.261	16.191	8.206	40.38
5	2.398	4.055	13.755	11.856	6.760	50.97
6	3.063	3.895	12.125	10.621	5.251	65.09
7	3.529	4.140	11.652	8.212	5.830	82.73
8	1.766	5.106	14.199	13.201	3.972	100.38
9	2.589	4.998	18.005	11.249	5.255	121.55
10	7.143	4.945	3.732	4.845	4.203	153.32

the entire range spanned by the predictions. There is a very good agreement in the mean droplet velocity comparisons at all locations.

Figs. 18a-d show the scatter plots of mean droplet radial velocity. As in the gas-phase, the experimental data show a great deal of turbulent fluctuations when it comes to measuring the radial velocities. The error bars based on the rms component clearly show that the fluctuations are very large and in some instances even exceed their corresponding mean. Again, the agreement is quite good at the first three axial locations. At the last location, the computations seem to underpredict the experimental data only in the inner region.

4.2 Case 3: A Confined Swirling & Reacting Spray Case[9]

For the third case, the schematic of the burner is shown in Fig. 19 which comprises of an air-assist atomizer located in the center surrounded by a co-flowing stream.[9] The flow rates were measured at a co-flow air rate of 12.10 g/s, an air-assist flow rate of 1.25 g/s and a liquid fuel flow rate of .30 g/s. The fuel used was n-heptane. Droplet size and velocity, and droplet number flux were reported at different axial locations starting from 2.5 mm. The velocity and droplet data were obtained by using a 2-component Phase/Doppler particle analyzer. The following uncertainties in the measurements were reported: ± 0.2 mm in position measurements, ± 10 % in mean droplet velocities, and ± 6.5 % in droplet sizes. Uncertainties in droplet flux measurements were not reported as its accuracy depends upon the aggregate of the individual accuracy of measurements in droplet velocity, size, and probe volume size.

The success of any spray model depends a great deal on the correct specification of the injector exit conditions. The liquid fuel injection was simulated by injecting a discretized parcel of liquid mass from the injector at the beginning of every fuel-injection time step. Table 1 summarizes the initial conditions used in the spray distribution. The table represents the integrated averages of the experimental measurements taken at the nearest axial location. And the initial
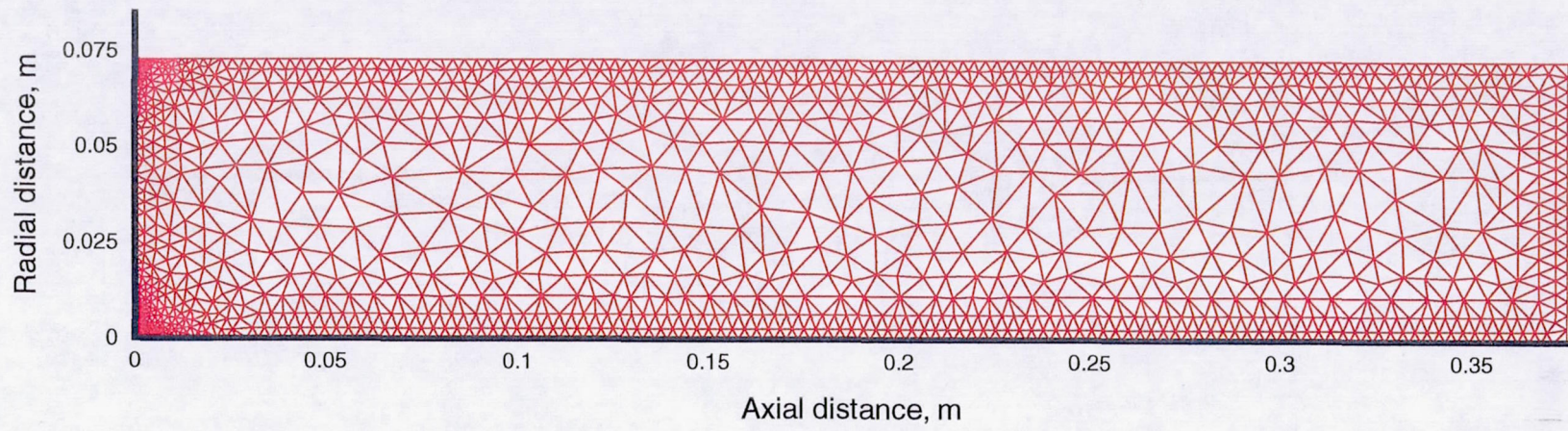
24

Fig. 20 Computational grid for Case 3, a reacting spray with swirl.

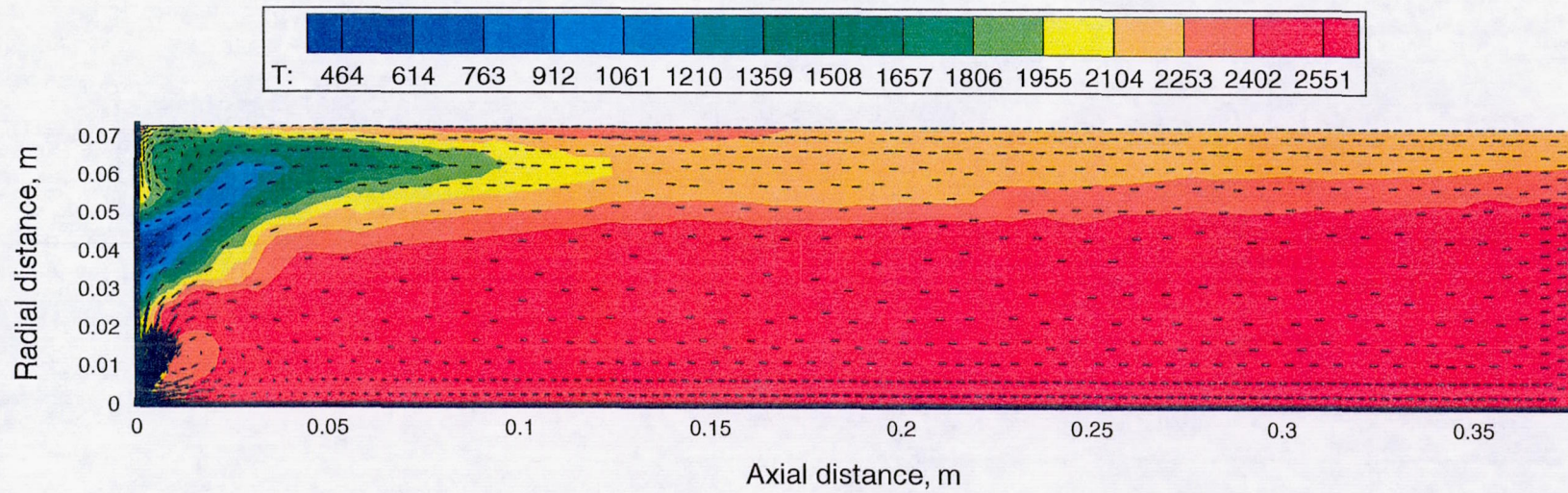T: 464 614 763 912 1061 1210 1359 1508 1657 1806 1955 2104 2253 2402 2551

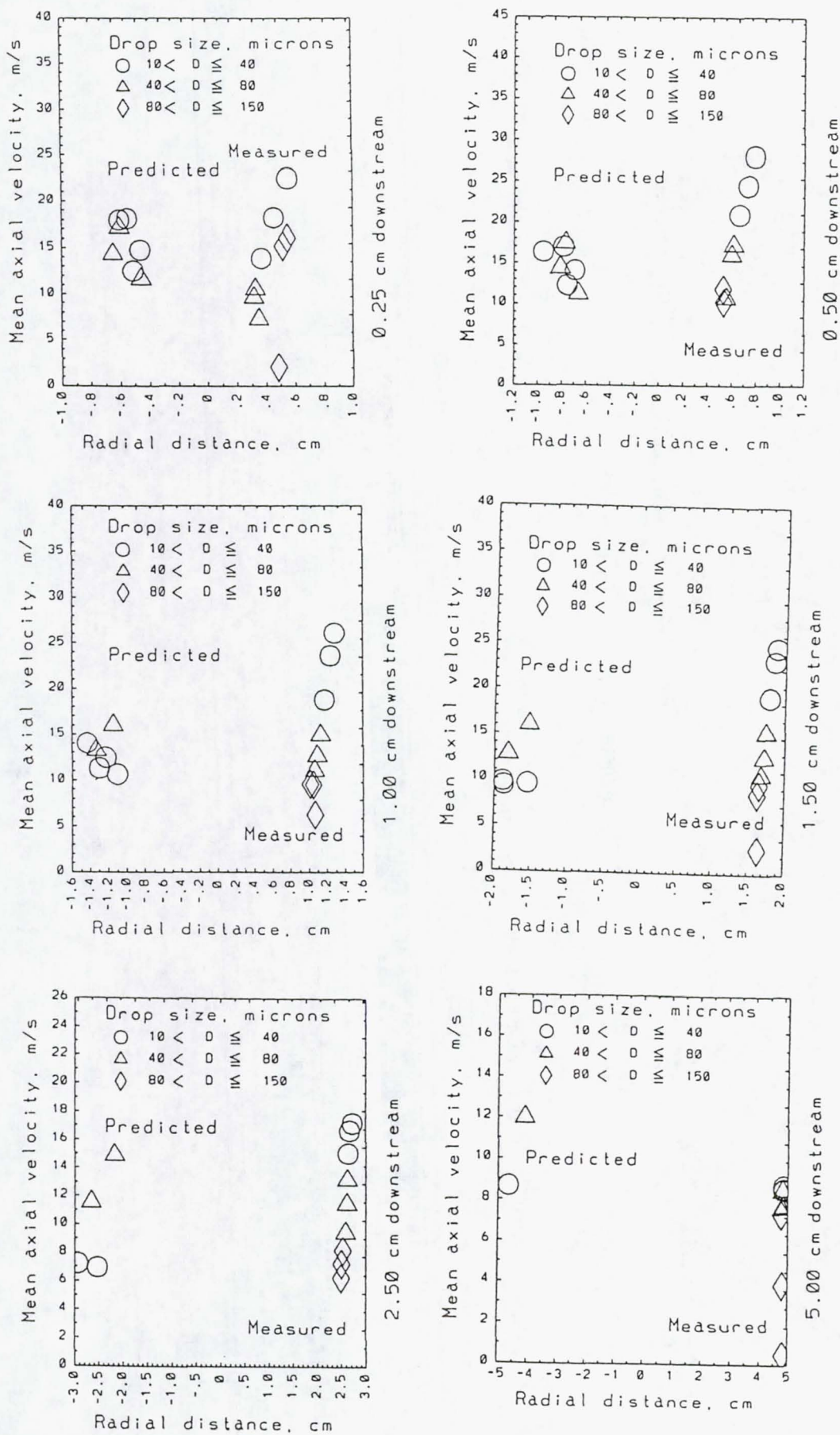Fig. 21 Gas-phase mean temperature distribution & velocity vector plot for Case 3.
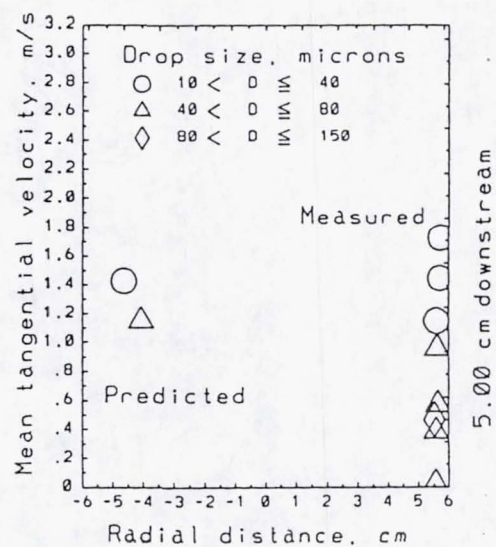
Fig. 22   Mean drop axial velocity comparisons for Case 3.

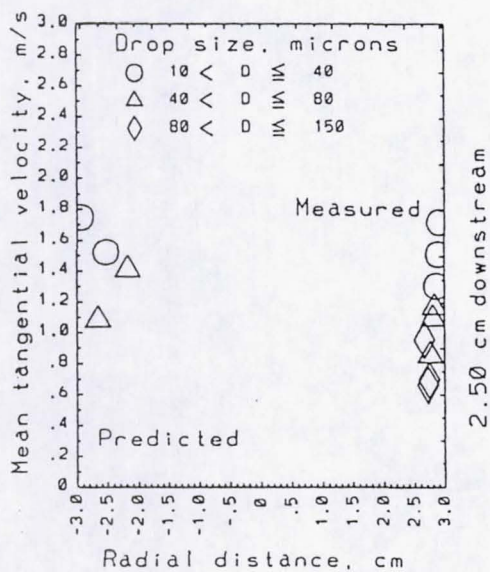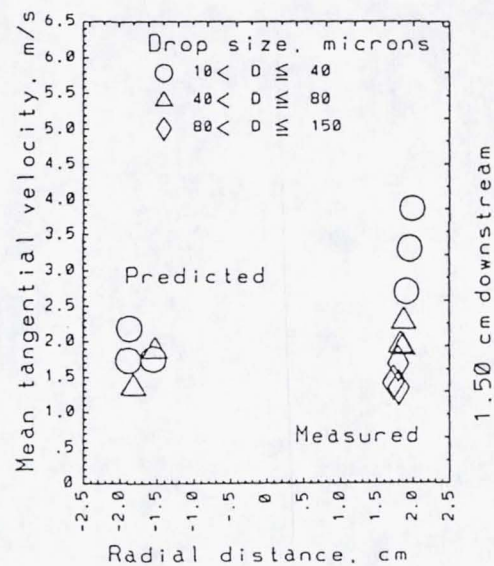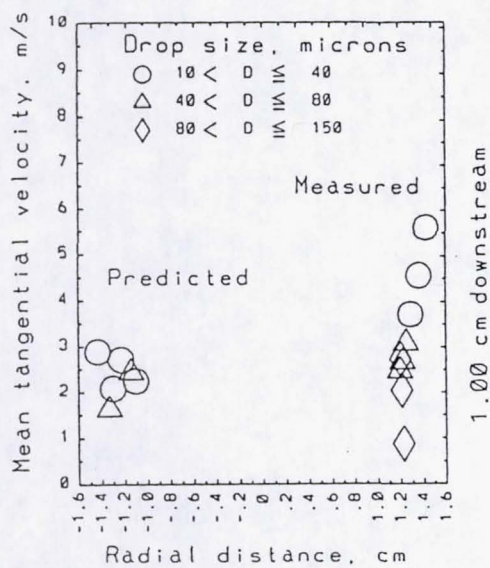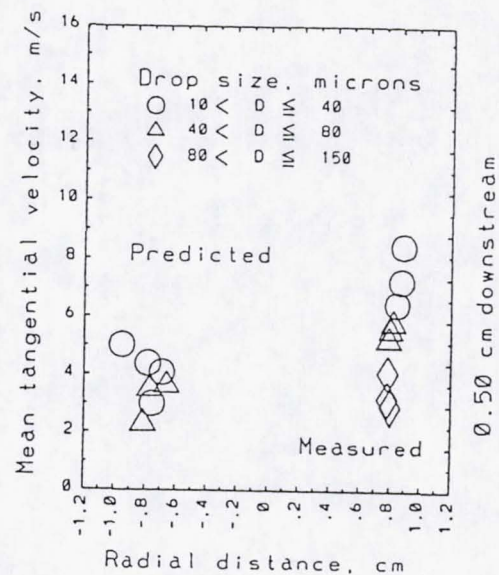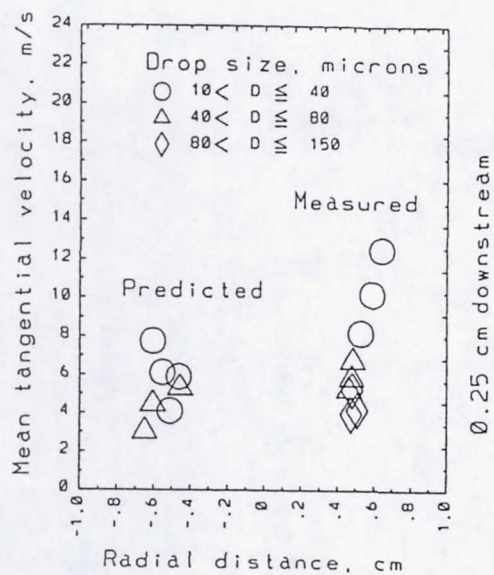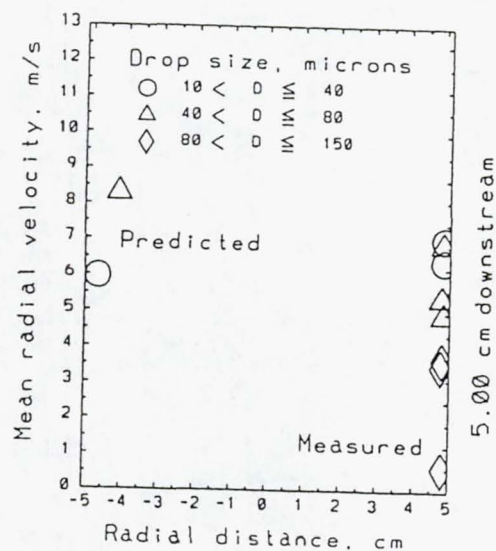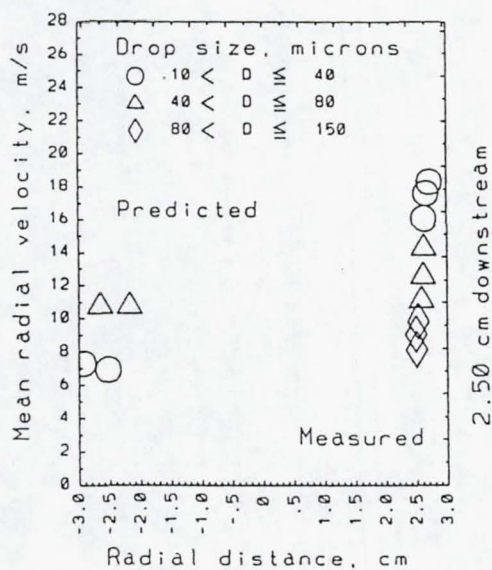Fig. 23   Mean drop tangential velocity comparisons for Case 3.
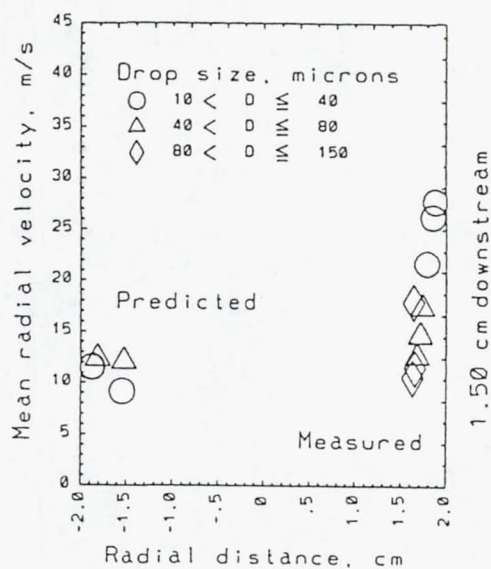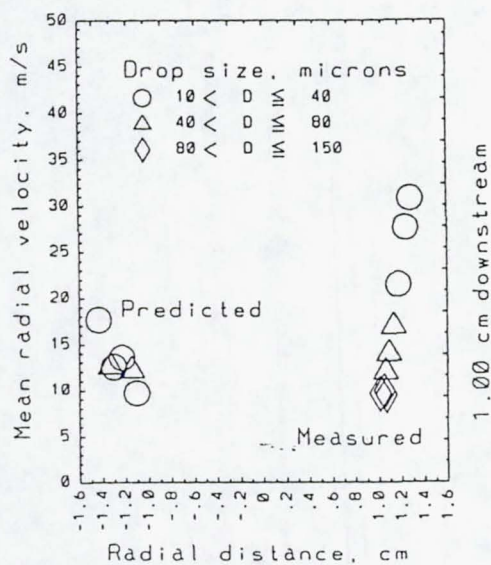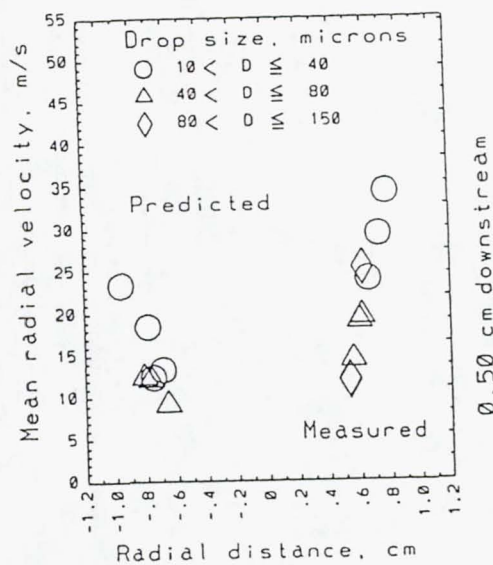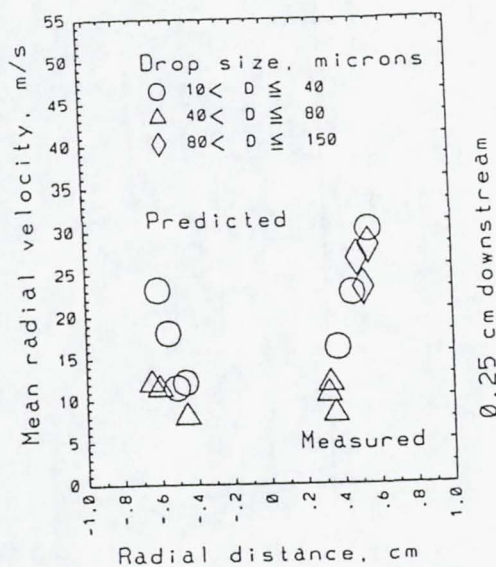
27

Fig. 24   Mean drop radial velocity comparisons for Case 3.

28

droplet temperature was assumed to be 300 K. Some measure of randomness in the initial droplet conditions is taken into account by assuming both r_{ko} and droplet velocities to have a mean as given by the values in Table 1 with a Gaussian distribution. The variance in r_{ko} is taken to be 35 % of its mean and for the droplet velocity to be 25 %.

Since no direct measurements for the gas velocity were reported, the specified inflow gas velocity was taken to be equal to the reported measurements of drop velocity for the smallest of drop sizes (four microns). In the absence of any reported measurements in temperature, the specified inflow temperature profile was assumed to be equal to the case of an open combusting spray reported in Ref. 10. And the composition of the inflow was taken to be that of air. The assumptions made in prescribing the inflow conditions would contribute an element of uncertainty to the validation for this case.

Two different sets of computations were performed for the same case with one on a grid of 2486 triangular elements and the other on a grid of 3600 quadrilateral elements. The turbulence Schmidt and Prandtl numbers were taken to have a value of 0.70. The PDF solution is obtained by making use of 100 particles per cell. The temperature and species fields supplied to the CFD and liquid phase solvers are obtained from averaging the PDF solutions over the previous 100 time-steps. The calculations were advanced until a steady state solution is reached by making use of the following time steps: Δt_g is determined based on a CFL number of 4, $\Delta t_{injection} = 1.0$ ms, and Δt_k = 0.01 ms. At the end of every liquid phase injection time step, a new spray distribution comprised of 10 different droplet groups was introduced.

The following results refer to the computations performed on a triangular mesh. The computational grid is shown in Fig. 20 and the temperature distribution is shown in Fig. 21. Fig. 21 shows that most of the combustion occurs in a region where a flame is stabilized by the swirl-induced recirculation.

Figures 22-24 show the comparisons for the mean drop axial, tangential, and radial velocities, respectively. The comparisons are shown for six downstream axial locations of 0.25, 0.5, 1.0, 1.5, 2.5 and 5.0 cm. Since the Lagrangian spray computations were performed by introducing only a few droplet groups representative of the measured droplet distribution, it is not possible to make direct one-on-one comparisons with the experimental data. The predicted droplet velocities and locations shown in the figures were ob-

tained by following the droplets as they traverse the axial location at which measured data are available. The measured data represent the mass-weighted integrated averages of both droplet location and velocities for drops of different sizes ranging from 10 to 150 microns. In the axisymmetric computations, one would expect to see a mirror image of identical representation on either side of the centerline. But in order to distinguish the symbols used for predictions from the measurements, the measured data is plotted to the right of the axis of symmetry and the predictions to the left. The radial distance in the figures varies from 1 to 6 cm in the downstream axial location indicating the extent of the radial spreading of the spray. The droplet spreading as evidenced by the radial locations of different droplet size groups, and the droplet velocity comparisons as evidenced from Figures 22-24 show good agreement at all six axial locations.

5 CONCLUDING REMARKS

The NCC solution procedure can capture the overall structure of a spray under both reacting as well as non-reacting conditions; and its application to several spray flames (both confined as well as unconfined) showed reasonable agreement with the available spray measurements. Ref. 1 provides a validation summary for some more additional cases with equally good comparisons. The solution procedure is based on the application of the scalar Monte Carlo PDF method with unstructured grids and parallel computing.

The detailed comparisons made for the case of a reacting spray illustrated the importance of chemistry/turbulence interactions in the modeling of a reacting spray. The PDF results were found to be closer to the reported experimental data when compared with the non-PDF solution. The PDF computations predict that most of the combustion occurs in a predominantly diffusion-flame environment. However, the non-PDF solution predicts incorrectly that the combustion occurs in a predominantly vaporization-controlled regime. The Monte Carlo temperature distribution showed that the functional form of the PDF for the temperature fluctuations varied substantially from point to point; on one end it showed a single peak near the flame temperature and on the other a single peak near the surrounding gas temperature. The results cast some ambiguity regarding the applicability of the widely used assumed-shape PDF methods in spray computations.

While the comparisons for the non-reacting spray were in reasonable agreement, the differences between the scalar Monte Carlo PDF method and the conventional methods were found to be negligible.

6 ACKNOWLEDGEMENT

7 REFERENCES

1. M.S. Raju, Application of Scalar Monte Carlo Probability Density Function Method For Turbulent Spray Flames, Numerical Heat Transfer, Part A, vol. 30, pp. 753-777, 1996.

2. M.S. Raju, Scalar Monte Carlo PDF Computations of Spray Flames on Unstructured Grids With parallel Computing, Numerical Heat Transfer, Part B, No. 2, Vol. 35, pp. 185-209, March 1999.

3. M.S. Raju, An Overview of the NCC Spray/Monte-Carlo-PDF Computations, AIAA 2000-0337, AIAA 38th Aerospace Sciences Meeting, Reno, Nevada, January 2000.

4. K.-H. Chen, A.T. Norris, A. Quealy, and N.-S. Liu, Benchmark Test Cases For the National Combustion Code, AIAA 98-3855, AIAA/ASME/SAE/ASEE 34th Joint Propulsion Conference, Cleveland, Ohio, July 13-15, 1998.

5. M.S. Raju, LSPRAY - A Lagrangian Spray Solver - User's Manual, NASA/CR-97-206240, NASA Lewis Research Center, Cleveland, Ohio, November 1997.

6. M.S. Raju, EUPDF - An Eulerian-Based Monte Carlo Probability Density Function (PDF) Solver - User's Manual, NASA/CR-1998-20401, NASA Lewis Research Center, Cleveland, Ohio, April, 1998.

7. M.S. Raju, Current Status of the Use of Parallel Computing in Turbulent Reacting Flows: Computations Involving Sprays, Scalar Monte Carlo Probability Density Function & Unstructured Grids, Advances in Numerical Heat Transfer, vol. 2, ch. 8, To appear.

8. V.G. McDonell and G.S. Samuelsen, An Experimental Data Base for the Computational Fluid Dynamics of Reacting and Nonreacting Methanol Sprays, J. Fluids Engineering, vol. 117, pp.145-153, 1995.

9. D.L. Bulzan, Velocity and Drop Size Measurements in a Confined, Swirl-Stabilized Combusting Spray, AIAA 96-3164, 32rd AIAA/ ASME/ SAE/ ASEE Joint Propulsion Conference, July 01-03, 1996/Buena Vista, FL.

10. D.L. Bulzan, Structure of a Swirl Stabilized, Combusting Spray, NASA Technical Memorandum: NASA TM-106724, Lewis Research Center, Cleveland, Ohio, 1994.

11. National Combustion Code, Version 0.9.0, Turbomachinery and Propulsion Systems Division, NASA Glenn Research Center at Lewis Field, Work in progress, July 11, 2000.

REPORT DOCUMENTATION PAGE

Form Approved
OMB No. 0704-0188

1. AGENCY USE ONLY *(Leave blank)*	2. REPORT DATE	3. REPORT TYPE AND DATES COVERED
	December 2000	Final Contractor Report

4. TITLE AND SUBTITLE

A Validation Summary of the NCC Turbulent Reacting/Non-Reacting Spray Computations

5. FUNDING NUMBERS

WU–708–28–13–00
NAS3–98008

6. AUTHOR(S)

M.S. Raju

7. PERFORMING ORGANIZATION NAME(S) AND ADDRESS(ES)

Dynacs Engineering Company, Inc.
2001 Aerospace Parkway
Brook Park, Ohio 44142

8. PERFORMING ORGANIZATION REPORT NUMBER

E–12558

9. SPONSORING/MONITORING AGENCY NAME(S) AND ADDRESS(ES)

National Aeronautics and Space Administration
Washington, DC 20546–0001

10. SPONSORING/MONITORING AGENCY REPORT NUMBER

NASA CR—2000-210600
AIAA–2001–0806

11. SUPPLEMENTARY NOTES

12a. DISTRIBUTION/AVAILABILITY STATEMENT

Unclassified - Unlimited
Subject Categories: 07, 20, 34, 61, and 64   Distribution: Nonstandard

Available electronically at http://gltrs.grc.nasa.gov/GLTRS

This publication is available from the NASA Center for AeroSpace Information, 301–621–0390.

12b. DISTRIBUTION CODE

13. ABSTRACT *(Maximum 200 words)*

This paper provides a validation summary of the spray computations performed as a part of the NCC (National Combustion Code) development activity. NCC is being developed with the aim of advancing the current prediction tools used in the design of advanced technology combustors based on the multidimensional computational methods. The solution procedure combines the novelty of the application of the scalar Monte Carlo PDF (Probability Density Function) method to the modeling of turbulent spray flames with the ability to perform the computations on unstructured grids with parallel computing. The calculation procedure was applied to predict the flow properties of three different spray cases: one is a nonswirling unconfined reacting spray, the second is a nonswirling unconfined nonreacting spray, and the third is a confined swirl-stabilized spray flame. The comparisons involving both gas-phase and droplet velocities, droplet size distributions, and gas-phase temperatures show reasonable agreement with the available experimental data. The comparisons involve both the results obtained from the use of the Monte Carlo PDF method as well as those obtained from the conventional CFD solution. Detailed comparisons in the case of a reacting nonswirling spray clearly highlight the importance of chemistry/turbulence interactions in the modeling of reacting sprays. The results from the PDF and non-PDF methods were found to be markedly different and the PDF solution is closer to the reported experimental data. The PDF computations predict that most of the combustion occurs in a predominantly diffusion-flame environment. However, the non-PDF solution predicts incorrectly that the combustion occurs in a predominantly vaporization-controlled regime. The Monte Carlo temperature distribution shows that the functional form of the PDF for the temperature fluctuations varies substantially from point to point. The results also bring to the fore some of the deficiencies associated with the use of assumed-shape PDF methods in spray computations.

14. SUBJECT TERMS

Combustion; Two-phase flows; CFD

15. NUMBER OF PAGES

36

16. PRICE CODE

A03

17. SECURITY CLASSIFICATION OF REPORT	18. SECURITY CLASSIFICATION OF THIS PAGE	19. SECURITY CLASSIFICATION OF ABSTRACT	20. LIMITATION OF ABSTRACT
Unclassified	Unclassified	Unclassified	